FATIGUE TESTING OF RIBBED ORTHOTROPIC PLATE BRIDGE ELEMENTS

by

H. L. Davis
A. A. Toprac

Research Report No. 77-1

Research Project Number 3-5-64-77 (HPR-1-4)

Fatigue Strength of Plate Girder Webs
Under Constant Moment

Conducted for

The Texas Highway Department
Interagency Contract No. 4413-938

In Cooperation with the
U. S. Department of Commerce, Bureau of Public Roads

by

CENTER FOR HIGHWAY RESEARCH
THE UNIVERSITY OF TEXAS
AUSTIN, TEXAS
May 1965

PREFACE

This is the first report in a series of reports to be written covering the work of this project. The reports are:

Report No. 1 - "Fatigue Testing of Ribbed Orthotropic Plate Bridge Elements" by A. A. Toprac and H. L. Davis; this report covers only the work performed on the orthotropic plate portion of the project concerned with the "Fatigue Strength of Plate Girder Webs Under Constant Moment."

ACKNOWLEDGEMENTS

The tests described herein were conducted as a part of the overall research program of the University of Texas Center for Highway Research under the administrative direction of Dean John J. McKetta. The work was sponsored jointly by the Texas Highway Department and the Bureau of Public Roads under an interagency contract between the University of Texas and the Texas Highway Department. Liaison with the Texas Highway Department was maintained through the advisory committee for this project consisting of Mr. Wayne Henneberger and Mr. Larry G. Walker. The study was directed by A. A. Toprac, Professor of Civil Engineering.

The authors would like to express their thanks to Mr. H. S. Lew and Mr. James S. Noel for their consultation in the development of testing methods and for suggestions for the presentation of this study.

TABLE OF CONTENTS

ABSTRACT

A test program of four full-sized sections of a proposed orthotropic steel deck plate bridge was initiated at the University of Texas to determine the fatigue strength of two different rib to deck plate connections and two types of field rib splices.

The ribs of the specimen were of the torsionally stiff trapezoidal shape design. Two of the specimens had a small flange at the upper edge of the ribs and were attached to the deck using a continuous fillet weld. The ribs of the other specimens were straight and were attached to the deck using a bevel weld. One of the rib splices consisted of a diaphragm plate that was fillet welded to the ribs. A butt weld and back up plate was used for the other splice.

The straight ribs attached with a bevel weld and the butt welded splice were found to be satisfactory. The flanged ribs and diaphragm plate splice were not satisfactory; however, test results indicate that these configurations may be made acceptable by incorporating slight modifications.

INTRODUCTION

A recent innovation in bridge construction is the use of cross-stiffened steel deck plates to replace conventional concrete decks. In this type of structure, which has become known as an "Orthotropic Steel Deck Plate Bridge," the deck plate serves as the upper flange for the ribs, the floor beams, and the main girders (Fig. 1). Such an arrangement of structural members results in a light-weight, **but highly redundant structure. This is in sharp contrast to the conventional** method of design in which the structural members are stacked one upon another and analyzed independently.

The first attempt to utilize orthotropic plate construction began with the introduction of the "battle deck floor" system in the 1930's (1).* This system was not particularly successful as the deck functioned only as the upper flange of the ribs and did not participate in the floor beam and main girder stresses.

It was not until the end of World War II that the first bridges were built in Germany using the deck plate as the upper flange of the floor beams and main girders. Such a design concept was prompted by the necessity of rebuilding a large number of bridges in spite of a severe steel shortage. The successful completion of the first few bridges built in the period of 1950-1954, examples of which are given in References 2 and 3, prompted the design and construction of many other orthotropic plate bridges both in Europe and elsewhere. Some outstanding examples

---

*Numbers in parenthesis refer to references listed on pages 21 and 22.

are the Save River Bridge in Belgrade, Yugoslavia, with its 856 foot span being the longest plate girder span in the world; and the Port Mann Bridge (4) in Vancouver, Canada, with a main arch span of 1200 feet.

The most common method of analysis used in the design of orthotropic plate bridges was developed by Pelikan and Esslinger (5) in 1957. This method consists of calculating the stresses in the structure assuming no deflection of the floor beams. The effect of floor beam deflection is then calculated and superimposed on the initial stresses. This method was developed as a practical solution to the differential equations of the orthogonal-anisotropic plate presented by Huber in 1914. (6, 7).

Other significant contributions to the design of orthotropic plates were made by Cornelius (8) in 1947 and by Mader (9). The design procedures developed by Cornelius and Mader were used in the design of the Save River Bridge. This method was not generally accepted due to its mathematical complexity.

As with all new structural concepts, a large amount of research was required to validate the theoretical analysis of the "orthotropic steel deck plate." The bulk of this research so far has been conducted in Europe, with the first tests of significance on both open rib and closed rib sections carried out respectively at the Technical University of Darmstadt in 1954 (10), and at the Technological University in Stuggart in 1957 (5, 11). Although these static tests validated the basic orthotropic plate theory for low loads, the ultimate capacity of the ribbed sections were found to be significantly greater than predicted by first order flexure theory.

Fatigue tests on open rib sections were conducted at Darmstadt in 1960 (12). These tests indicated that the fatigue strength of the deck and ribs approached the yield stress of the material. It cannot be

assumed, however, that the same is true for closed rib sections.

Fatigue tests on closed ribbed specimens have been conducted by Hansch and Muller (13, 14). These tests are only useful, however, in evaluation of rib splices.

A literature survey on the subject of orthotropic plates disclosed that no experimental data is available from laboratories in the United States. In order to build up experience in this type construction, a research project was initiated at The University of Texas by the Texas Highway Department. The data obtained from this project is to be used in conjunction with a proposed experimental bridge.

The purpose of the test program presented in this report was to determine the fatigue strength of several of the weld details of a deck stiffened with closed trapezoidal ribs. More specifically, the details examined were:

1) Rib to deck plate connection (Fig. 2)
    a. Bevel welded "straight" ribs
    b. Fillet welded flanged ribs
2) Field Rib Splice (Fig. 3)
    a. Fillet welded diaphragm plate
    b. Butt weld with back up plate

Both the bevel welded rib to deck connection and the butt welded rib splice have been previously proven as acceptable designs with high fatigue strength. The other two appeared to have fabrication advantages over the former, and could produce significant cost savings in future structures, if they were proved to have satisfactory fatigue strength.

TEST SET-UP AND PROCEDURE

Description of Specimen

The specimens consisted of two closed trapezoidal ribs welded to the under side of a deck plate. ASTM A36 steel was used for both the deck plate and ribs. The thickness of the deck and rib plate was 7/16 inch and 1/4 inch respectively. The results of laboratory coupon tests for the static yield point and other mechanical properties of the plates are given in Table 1. Mill test results are shown in Table II. The actual thicknesses of the plates used in the fabrication of the specimens and the calculated section properties of the test specimens are given in Table 3.

The test specimens were each 18' -0" long with the main bearing points at 12' -6" centers and a 5' -6" overhang. The general configuration of the specimens is shown in Fig. 2. Detail drawings are given in Fig. 4. The specimens represented full-size sections of a proposed bridge.

All specimens were identical except for the details of the rib to deck plate connection and the rib and deck splices in one of the specimens. Two types of rib to deck connections were used. In two of the specimens the ribs were fabricated with a small flange at the upper edge. The ribs were then attached to the deck using a continuous fillet weld between the rib flange and deck. The ribs of the remaining specimens were not flanged and were attached to the deck using a bevel weld (Fig. 2).

The specimen in which the rib and deck splices were located was of the unflanged or straight type. Details of the rib splices are shown in Fig. 3. Deck splice details are shown in Fig. 4. The rib splice initially consisted of a diaphragm plate that was continuously welded to both ribs. Upon completion of testing of the diaphragm splice, a 3" length of the

specimen containing the splice was removed and the specimen was re-spliced using a belt-type field splice and back-up-plate inside the rib. The back-up-plate was left in place and all welds ground smooth.

Two types of electrodes were used for welding (AWS E7018 and E6010). On each specimen one rib was completely welded to the deck using only one type of electrode while the other rib was welded using only the other type. The welding procedures used were approved by the Texas Highway Department.

Test Set-Up

The test set-up (Fig. 5) was devised so that the critical stresses were produced primarily by the local loads on the deck rather than by overall flexure of the specimen. This was accomplished by providing continuity over the interior support, thus reducing the bending moment in the span. The test set-up also closely approximated actual field conditions. Figure 6 is a photo of one of the specimens under test.

The main bearing points on which the specimen was supported were at 12'-6" centers with the roller support in the interior. The support at the overhang was located 5'-6" from the interior support and was used to prevent the overhanging end from deflecting upward, thus providing the desired continuity over the interior support. Both the main bearing supports and the overhang support were fastened to the laboratory test slab.

The load was applied at the center of the long span using a general purpose test cylinder. This cylinder, with a maximum capacity of 160 kips static and 120 kips dynamic, was used for both the static and cyclic loading.

The applied load was distributed over a 24" x 12" area using a two inch thick, 60 durometer, butyl pad which could easily deform to follow the

deflected shape of the specimen. An eight inch WF beam was used to distribute the jack load over the 24 inch length of the load pad. A 5/8" steel plate was placed between the butyl pad and the 8 inch beam to prevent local failure of the pad.

Test Procedure

As the results of the tests could not be accurately predicted, it was decided to continuously modify the applied loads and loading sequence as the test progressed rather than preplan a set test program. After cracks developed in the welds, the specimens were repaired using a procedure approved by the Texas Highway Department. The maximum cyclic load was then reduced and the specimen retested. This procedure allowed optimum utilization of the specimens.

All loads used are expressed in terms of 16 kip wheel loads plus a 30% impact factor. The frequency of the applied cyclic load was about 250 cycles per minute for all specimens. Each specimen was tested statically prior to fatigue testing. Static tests were also run periodically during the fatigue testing to determine if any changes had occurred in the flexural stiffness of the specimen as a result of the cyclic loading. The load increment used in the static tests was 8,000 lbs.

Two of the specimens were statically loaded to failure upon completion of fatigue testing.

Instrumentation

The instrumentation for the tests included measurements of deflections and strains of the ribs and deck plate. Local strains under and near the applied load were also measured. The specimens were also white washed so that the type and location of yielding could be determined.

The instrumentation used on Specimens 2 and 3 was more extensive than that used on Specimens 1 and 4. Strain and deflection measurements were made only during static tests.

Vertical deflections were measured using 0.001 inch dial indicators. The location of the gages are shown in Fig. 7. Deflections were measured on both the ribs and deck plate. Dial gages were also located at the overhang support to measure any upward deflection of the support. No attempt was made to measure the residual deflection, if any, as the fatigue testing progressed.

Electrical strain gages were used for strain measurements. All gages used had a nominal length of 1/2 inch. The location of the strain gages is shown in Fig. 8.

TEST RESULTS

The test results for each specimen are described below, with the fatigue and ultimate load tests being presented separately.

Fatigue Tests

Specimen 1. The first specimen tested was of the flanged rib type. Prior to fatigue loading this specimen was tested statically to a load of 83.0 kips which produced an average pressure under the load pad of 288 psi.* This load was equivalent to 4.0 times a 16 kip wheel load plus a 30% for impact (15). As there were two ribs on the specimen, each rib carried two wheel loads, or approximately twice the expected maximum load on the rib. Experimental stresses and strains measured during the static test are shown in Fig. 9. Measured deflections are shown in Fig. 10. Extensive yielding, as indicated by measured strains and observed yield lines, occurred directly under the load and on the inner walls of both ribs at the bend line of the rib flange. The magnitude of the measured stresses at the lower faces of the ribs indicated that yielding should have occurred; however, the strains remained linear and no yield lines were observed.

The fatigue testing history of the specimen is shown in Fig. 10. The initial cyclic load fluctuated between 8.3 kips and 83.0 kips. After 10,000 cycles at this load level a 16 inch crack (1)** was formed in the weld between the rib flange and the deck. The crack, which had developed

---

*Attention was paid to the magnitude of this pressure as it was considered as one of the parameters by other investigators. According to the AASHO Specification (15) such pressure is 66.7 psi for an H-20 truck loading plus 30% impact.

**Circled numbers are used to identify cracks indicated in Figure 10.

in the rib welded with the E7018 electrode (west rib) was located on the flange of the rib inner wall (flange closer to longitudinal axis of symmetry) (Fig. 11) and extended symmetrically from the load point. Extensive yielding had also occurred on the lower face and inner wall of both ribs as indicated by yield lines on the specimen.

The crack was repaired and testing resumed using a maximum load of 49.0 kips and a minimum load of 9.0 kips. The average pressure under the load pad for the maximum load was 170 psi. After an additional 35,000 cycles an 8 inch crack (2) was noted at the same location as the previous crack. Testing was continued and after 240,000 cycles, the crack stabilized at its maximum length of 26 inches.

A similar crack (3) developed in the rib welded with the E6010 electrode (east rib) after one million cycles. This crack was four inches long when observed and did not propagate. Another crack (4) developed also at this time at the intersection of the lower face of the west rib and the vertical plate at the interior support (Fig. 12). This crack was due to flexure of the vertical plate as compression stresses existed in the lower face of the rib in this negative moment region. This crack did not propagate and had no effect on the stiffness of the specimen.

Testing was continued and at 1.5 million cycles a new crack (5) developed at the bend line of the rib flange of the west rib directly under and parallel to the initial crack in the weld. (Fig. 11). This crack eventually grew to a length of 24 inches after 2 million cycles. A crack (6) at the intersection of the lower face of the east rib and the vertical plate at the interior support was also noted at 1.5 million cycles.

Testing was terminated after 2 million cycles. Results of a static test performed at the conclusion of the fatigue test indicated no appreciable

change in the stiffness of the specimen in spite of the cracks.

Specimen 2. The second specimen was also of the flanged type. A maximum load of 49.0 kips was used for the initial static test. The experimental stresses and strains are shown in Fig. 13. Measured deflections are shown in Fig. 14. Yielding was not indicated either by the measured strains or by yield lines on the specimen.

The loads and loading sequence used in the fatigue testing are shown in Fig. 14. The initial cyclic load fluctuated between 40.0 kips and 9.0 kips. After 20,000 cycles at this load a six inch crack was noted at the same location as the initial crack on Specimen 1. As this specimen was to be tested to ultimate, testing was terminated after 36,000 cycles so that excessive cracks would not be formed in the specimen.

Specimen 3. This specimen was of the non-flanged type. In order to obtain an accurate comparison between the flanged and unflanged specimens, this specimen was tested using the same sequence of loading as the first flanged specimen.

The initial static test load was again 83.0 kips. Experimental stresses and strains are shown in Fig. 15. Deflections are shown in Fig. 16. Extensive yielding occurred directly under the load pad; however, unlike the first flanged specimen, no yielding was in evidence at the upper edge of the rib inner walls.

The fatigue testing history of the specimen is shown in Fig. 16. The initial load fluctuated between 83.0 kips and 8.3 kips. After 10,000 cycles the load was changed to fluctuate from 49.0 kips and 9.0 kips. At this time a few yield lines had appeared on the lower faces of the ribs, but no weld cracks were observed. After 980,000 cycles a crack developed in the weld at the intersection of the lower face of the west rib and the

vertical plate at the interior support. (Fig. 12). A similar crack developed in the opposite rib after 1.4 million cycles. As with the first specimen, these cracks did not propagate and had no influence on the stiffness of the specimen.

The test was terminated at 2 million cycles. The final static test, which was an ultimate load test, indicated no change in the flexural stiffness of the specimen as a result of the cyclic loading.

Specimen 4. This specimen was the non-flanged specimen in which the rib splice was located. The first rib splice evaluated was the fillet-welded diaphragm plate (Fig. 3). A maximum load of 49.0 kips was used for the initial static test. Experimental stresses and strains measured in the static test are shown in Fig. 17. Deflections are shown in Fig. 18. No yielding was indicated either by measured stresses or yield lines on the specimen.

The fatigue testing history of the specimen is shown in Fig. 18. A load that fluctuated between 49.0 kips and 9.0 kips was used for the fatigue test. After 7,300 cycles the weld in the tension region of both rib splices had completely failed. The weld was repaired and the specimen retested with a fatigue load that fluctuated between 29.8 and 9.0 kips. Failure again occurred in the rib splices after 107,000 cycles.

The diaphragm splice, as previously mentioned, was then cut completely out and the specimen respliced using the butt weld splice (Fig. 3). At a load of 40.0 kips which was used for the static test, a large number of yield lines appeared on the specimen. This yielding was attributed to residual stresses produced during the resplicing operation.

The specimen was then tested in fatigue for 2 million cycles with a load that fluctuated between 29.8 and 9.0 kips. As no additional

yielding or cracking occurred, the specimen was then fatigue tested for 100,000 cycles using a load that fluctuated between 40.0 kips and 9.0 kips and then for additional 100,000 cycles with a fluctuating load of 49.0 kips to 9.0 kips. The test was then terminated without any weld cracks having occurred.

Ultimate Load Tests

Specimen 2. This is the second flanged specimen that had previously been tested in fatigue. The six inch crack in the weld line mentioned in the discussion of the fatigue testing of this specimen was not repaired prior to the ultimate load test. The repair of the weld was not considered necessary as the results of the static tests on the first flanged specimen indicated no appreciable change in the stiffness of the specimen as a result of minor weld cracks.

The load was applied in 16.0 kip increments. Significant tension yielding was first noted under the load pad at a load of 64 kips. (Fig. 19). The maximum tensile stress calculated from measured strains at this load was 57,000 psi, considerably above the yield value indicated by coupon testing. This apparent yield load was also appreciably higher than the load required to produce yielding in the initial static test (Fig. 13). The difference in yield strengths could be due to strain - hardening from the initial static test (16). Tension yielding began on the lower faces of the rib at a load of 80.0 kips (Fig. 20). However, yield lines were not observed until the load reached 96.0 kips. The maximum measured tensile stress on the rib at the 80.0 kip load was 39,800 psi Also at a load of 80 kips tension yielding began to occur on the rib inner walls (Fig. 21). However, no yielding was observed on the rib outer walls. Compression yielding on

the top side of the deck plate in the area immediately adjacent to the load pad also began to occur at this load (Fig. 22, 23). As the load was increased beyond this point, yielding began on the outer walls of the ribs, and the inner walls of the ribs began to buckle outwards (Fig. 24). This buckling became quite extensive at the ultimate load (Fig. 25).

Buckling of the deck plate occurred at a load of 152.0 kips. The deflections of the specimen became uncontained at this time and the specimen was considered to have reached its ultimate load capacity (Fig. 26). Considerable compression yielding had occurred in the upper compression portion of the ribs (Fig. 27). The depth of these yield lines indicated that the neutral axis had moved considerably downward from its initial position, characteristic of a compression failure. Large permanent deformations had occurred directly under the load pad.

Specimen 3. This is the first unflanged specimen that had been previously tested in fatigue. The two small cracks previously described in the discussion of the fatigue test were not repaired as they had no effect on the flexural stiffness of the specimen. The load was applied in 8.0 kip increments.

At the previous maximum load (83.0 kips) used during the fatigue test, yielding began to occur under the load pad as indicated by observed yield lines and measured strains (Fig. 19). Similar to Specimen 2, this extremely high apparent yield point can be attributed to unloading from a yield condition during the initial static test (Fig. 15). Tension yielding also began to occur on the lower faces and inner walls of the ribs at this load (Figs. 20, 21). Yielding began on the outer faces of the ribs at a slightly higher load.

As the load was increased from this point, the area of the ribs which had yielded in tension began to grow quite rapidly and at a load of

128.0 kips had moved up to the calculated neutral axis and extended one foot on either side of the load line (Fig. 28). Unlike the flanged specimen, there was no indication of buckling of the inner rib walls.

Compression yielding on the upper side of the deck plate in the area adjacent to the load pad began at a load of 112.0 kips (Fig. 22). This yielding was similar to that on the flanged specimen, but not as extensive.

Cracks were observed in the weld line between the deck and the rib inner wall at a load of 128.0 kips. These cracks were each six inches long and located at the load point.

The load was then increased to 160.0 kips, the maximum capacity of the loading jack. The deflections of the specimen (Fig. 26) were still contained and failure was not considered to have occurred. At this load the tension yield lines on the ribs had moved upward to nearly the full height of the ribs indicating an upward shift in the neutral axis. This shift of the neutral axis was also indicated by a decrease in the compression stresses in the upper edge of the ribs (Fig. 24).

Considerable local deformation occurred at the load point but there was no indication of compression buckling of the deck.

DISCUSSION OF RESULTS

The results obtained in the test program are discussed below. As the specimens tested had a large ratio of span length to width, they resembled beams rather than plates which makes a direct comparison between the experimental results obtained and results obtained in other experimental investigations of orthotropic plates extremely difficult. However, as pointed out in the test objectives (page 3), the purpose of the test program was to obtain a relative comparison between different fabrication details rather than to attempt to validate orthotropic plate theory. Accordingly, the following discussion primarily consists of comparisons of one type of specimen with the other type. In areas where elementary theory is applicable, theoretical values have been calculated and compared with test results. The only instance in which the results of other investigations were found to be on a comparable basis with the results of this program is in the evaluation of the rib splice. The results of the initial static tests, fatigue tests, and ultimate load tests are discussed separately.

Static Tests

On all specimens, static tests were performed prior to and during the fatigue testing. The results of these static tests were found to be independent of the accumulated number of cycles on the specimen. Even in the specimens which had relatively large weld cracks there was found to be no appreciable change in the stiffness of the specimen.

The maximum tensile stresses in the deck were located on the lower side of the deck plate at the load point. The stresses measured at this location on the flanged specimen were found to be about 10% higher

than those measured on the unflanged specimen (Fig. 29). However, the measured stresses for all specimens agreed well with the theoretical value for this stress calculated in Appendix III. The effects of both transverse and longitudinal load distribution were used in the calculation of the theoretical stress; however, transverse stiffness was assumed to be furnished only by the ribs. This analysis procedure was found to be much simpler than the method presented in the AISC Manual (17).

The measured stresses on the lower faces of the ribs at the load point were in close agreement for the flanged and unflanged specimens (Fig. 30); however, the measured values were 10 to 15 per cent higher than the theoretical values calculated in Appendix II. The theoretical stress was calculated without considering transverse load distribution which accounts for the discrepancy between the calculated and measured values. The stresses at this point represented the approximate maximum tensile stresses which occurred on the ribs.

As the one-quarter point is a relatively large distance from the load point, the effect of transverse load distribution is negligible and the stresses measured at this point represent beam flexural stresses. As was expected, the measured stresses on the flanged and unflanged specimens were almost identical (Fig. 31) and agreed extremely well with the calculated beam bending stresses (Appendix II).

The experimental deflections of the rib at the load point are compared with the calculated deflections in Fig. 32. The deflections of the unflanged specimens were slightly larger than those of the flanged specimen. All measured deflections were significantly larger than the theoretical deflections calculated in Appendix II. The discrepancy between the measured and calculated values is probably due to the effects of local deformations in the loaded area. As the specimens had negligible

transverse stiffness, the experimental deflections cannot be compared to deflections in an actual orthotropic steel deck.

Fatigue Tests

A summary of the results of the fatigue tests is given in Table 4. In this table the fluctuating loads are expressed in terms of equivalent H-20 wheel loads (15). For the specimens tested, the fluctuating loads representing 1.50 and 1.93 H-20 wheel loads give the best approximations to actual design loads.

The flanged specimens were found to have a very low fatigue strength. In every case, failure of the weld between the rib flange and deck occurred at a very low number of cycles. This was in sharp contrast to the behavior of the unflanged specimens in which no fatigue cracks occurred in the rib to deck welds. Sufficient test data is not available to accurately determine the exact conditions that resulted in the low strength of the flanged specimen; however, a possible explanation is shown in Fig. 33. In the load equilibrium shown the bending moment transmitted across the vertical leg of the weld would produce tensile stress of sufficient magnitude to produce a fatigue failure in the weld at a low number of cycles. This failure would occur along the vertical leg of the weld which agrees with the actual test results.

The fatigue strength of the fillet welded diaphragm plate rib splice was found to be quite low. In every case, the failure occurred in the weld and initiated at the point of maximum tensile stress (lower face of rib). In Fig. 34 the results obtained in this investigation are compared with those in a similar investigation (see sketch in Fig. 34) conducted by Hansch and Müller (13, 14). The discrepancies between the results of the investigations are probably due to differences in the electrodes and welding procedures used. In both

investigations, the results indicate that the fatigue strength of the diaphragm plate splice is inadequate for use in the expected stress ranges.

As expected, the butt welded splice was found to have a satisfactory fatigue strength. The results of many investigations on butt welded joints also indicate the high fatigue strength of this type of configuration.

Ultimate Load Tests

There was little similarity between the behavior of the two types of specimens at extremely high loads. Failure of the flanged specimen was produced by buckling of the deck plate and rib inner walls. Buckling did not occur in the unflanged specimen at the maximum applied load, and this specimen was not considered to have failed.

The buckling of the rib inner walls on the flanged specimen can be directly attributed to the eccentricity of the load on the rib flange with the axis of the rib wall (Fig. 33). This eccentricity produced a local moment in the upper section of the rib inner wall which resulted in local compression yielding at relatively low loads (Fig. 24). As the load was increased further, the compression strains became large enough to produce buckling of the rib walls. The high local moments were not in evidence on the unflanged specimen as there was no eccentricity of the load on the rib walls. In fact, the compression strains on the unflanged specimen decreased at high loads as a result of an upward shift of the neutral axis resulting from extensive yielding in the tension area of the rib.

The strains measured on the deck plate (Fig. 22) indicate that both specimens had the same load distribution characteristics in the area in which buckling of the deck occurred. As the measured strains were slightly higher on the flanged specimen,there exists the possibility that

deck buckling of the unflanged specimen might also have occurred if a larger load had been applied. Deck buckling would not be expected in an actual orthotropic steel deck plate in which there are no free edges.

CONCLUSIONS AND RECOMMENDATIONS

Through this project valuable information was obtained on the general behavior of ribbed orthotropic plates, and data was collected in accordance with the objectives of the program.

Based on the results of the tests, the following conclusions can be drawn:

1. Flanged rib design was found to be unsatisfactory because of low fatigue strength.
2. The low fatigue strength exhibited by the specimens with flanged ribs is due to the propensity to cracking of the fillet weld between the deck and rib flange.
3. The fatigue strength of the unflanged specimens was satisfactory.
4. Butt-welded rib splices with a back-up plate proved to be satisfactory.
5. Diaphragm plate splices with a fillet weld detail used in this investigation proved to be unsatisfactory. This, however, does not mean that diaphragms may not prove satisfactory if different weld details were used.
6. The cracks which occurred in the rib flange to deck welds were found to have little or no influence on the flexural stiffness of the specimens. Because of this behavior, it is possible to reduce the amount of welding between the deck and the ribs.

Since the test loads used were larger than design loads, it seems reasonable to assume that a compromise between the two configurations (flanged and unflanged) could be developed that will prove to have satisfactory fatigue life and also be economical. It is recommended that this be investigated in the future. Since diaphragm splices are economical, their fatigue life at low bending stress regions should be investigated.

REFERENCES

1. American Institute of Steel Construction, The Battle Deck Floor for Highway Bridges, New York, 1938.

2. Schussler, K. and Pelikan, W., "Die Neue Rheinbrucke Koln-Mulheim," Der Stahlbau, vol. 20, 1951, p. 141.

3. Mayer, R., "Die Kurpfalzbrucke uber den Neckar in Mannheim," Der Stahlbau, vol. 27, 1952, pp. 85, 117 and 146.

4. Engineering News Record, "Novel Deck Saves Steel Weight," June 16, 1960, p. 47.

5. Pelikan, W. and Esslinger, M., "Die Stahlfahrbahn, Berechnung und Konstrucktion," M.A.N. Forschungsheft, No. 7, 1957.

6. Huber, M. T., "Die Grundlagen Einer Rationellen Berechnung der Kreuzweise Bewehrten Eisenbetonplatten," Zeitschrift des Osterreichischen Ingenieur und Architekten Vereines, vol. 66, 1914, p. 557.

7. Huber, M T., "Die Theorie der Kreuzweise Bewehrten Eisen Betonplatten," Der Bauingenieur, vol. 4, 1923, pp. 354-392.

8. Cornelius, W., "Der wirtschaftliche Entwurf der Stahlplattenfahrbahn (Orthotrope Platte)," Die Neue Koln-Mulheimer Brucke, p. 95, Herausgegeben von der Stadt Koln, 1951.

9. Mader, F. W., "Die Berucksichtigung der Diskontinuitat bei der Berechnung Orthotroper Plannen," Der Stahlbau, vol. 26 (1957), p. 283.

10. Kloppel, K., "Uber Zulassige Spannungen im Stahlbau," Stahlbautagung, Baden-Baden, 1954.

11. Pelikan, W., "Die Orthotrope Platte der Stahlfahrbahn," Stahlbautagung, Heidelberg, 1958.

12. Kloppel, K. and Roos, E., "Statische Versuche und Daverversuche Zur Frage der Bemessung von Flachblechen in Orthotropen Platten," Der Stahlbau, vol. 29, 1960, p. 361.

13. Hansch, H. and Muller, G., "Dauerfestigkeitsversuche an geschweiften Hohlrippenanschlussen," Der Stahlbau, vol. 31, 1962, p. 90.

14. Hansch, H., and Muller, G., "Dauerfestigkeitsversuche an Geschweiben Hohlrippenanschlussen," Schweisstechnik 11 (1961), H. 5, s. 143/98.

15. American Association of State Highway Officials, Standard Specifications for Highway Bridges, Eighth Edition, 1961.

16. Beedle, L. S., Plastic Design of Steel Frames, John Wiley and Sons, New York, 1958.

17. American Institute of Steel Construction: Design Manual for Orthotropic Steel Plate Deck Bridges, 1963.

18. Roark, R. J., Formulas for Stress and Strain, Third Edition, McGraw Hill Publishing Company, 1957.

TABLE I. Coupon Test Results

Specimen	Part	Yield Strength psi	Ultimate Strength psi	% Elongation
1	Deck	37,100	64,400	29.0
2	Deck	37,100	64,400	29.0
3	Deck	37,400	64,500	28.3
4	Deck	37,400	64,500	28.3
All	Ribs	40,700	64,700	26.8

TABLE II. Mill Test Results

Spec.	Part	Yield Strength psi	Ultimate Strength psi	% Elongation	Chemical				
					C	M_n	P	S	S_1
1	Deck	49,600	71,100	21.7	.23	.46	.010	.013	.06
2	Deck	49,600	71,100	21.7	.23	.46	.010	.013	.06
3	Deck	47,000	67,600	27.0	.11	.42	.016	.015	.07
4	Deck	47,000	67,600	27.0	.11	.42	.016	.015	.07
All	Ribs	46,800	68,800	25.7	.22	.57	.010	.019	.08

TABLE III. Section Properties

Property	Flanged	Unflanged
I in^4	575.2	569.5
$c_{(u)}$ in	2.89	2.95
$c_{(l)}$ in	9.07	9.00
A in^2	36.40	35.35
^1A_s in^2	12.38	12.38
^2K in^4	229.0	229.0
Rib thickness (in.)	.262	.262
Deck thickness (in.)	.456	.456

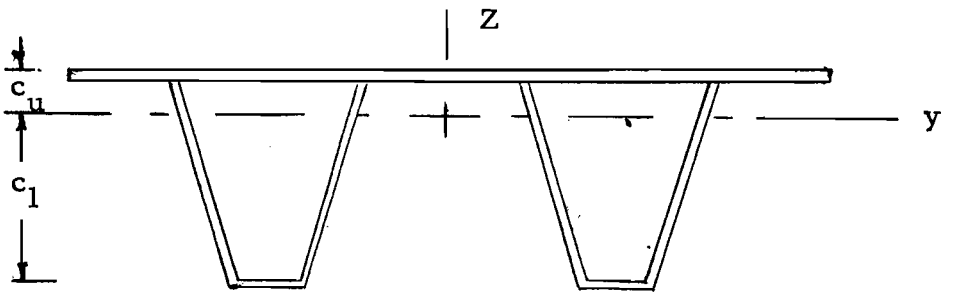

1 Area of vertical portion

2 For one rib

TABLE IV. Fatigue Test Results

Specimen No.	Type	Test No.	Pmax kips	Pmin kips	Equivalent Wheel Loads[b] Pmax	Pmin	(load range) Pmax - Pmin	Cycles[a]
1	Flanged	1	83.0	8.3	4.00	.40	3.60	10,000[c]
		2	49.0	9.0	2.36	.43	1.93	2×10^6 [d]
2	Flanged	3	40.0	9.0	1.93	.43	1.50	36,000[c, e]
3	Straight	4	83.0	8.3	4.00	.40	3.60	10,000
		5	49.0	9.0	2.36	.43	1.93	2×10^6
4	Straight Diaphragm Splice	6	49.0	9.0	2.36	.43	1.93	7,300[c]
		7	29.8	9.0	1.43	.43	1.00	107,000[c]
	Belt Type Splice	8	29.8	9.0	1.43	.43	1.00	2×10^6
		9	40.0	9.0	1.93	.43	1.50	100,000
		10	49.0	9.0	2.36	.43	1.93	100,000

a Total number of cycles at a given load
b Based on H-20 Truck Load plus 30% impact or 16 + 0.3 x 16 = 20.8 kips
c Weld failure occurred at number of cycles shown
d First weld failure at 35,000 cycles; testing not interrupted
e Weld failure at 20,000 cycles

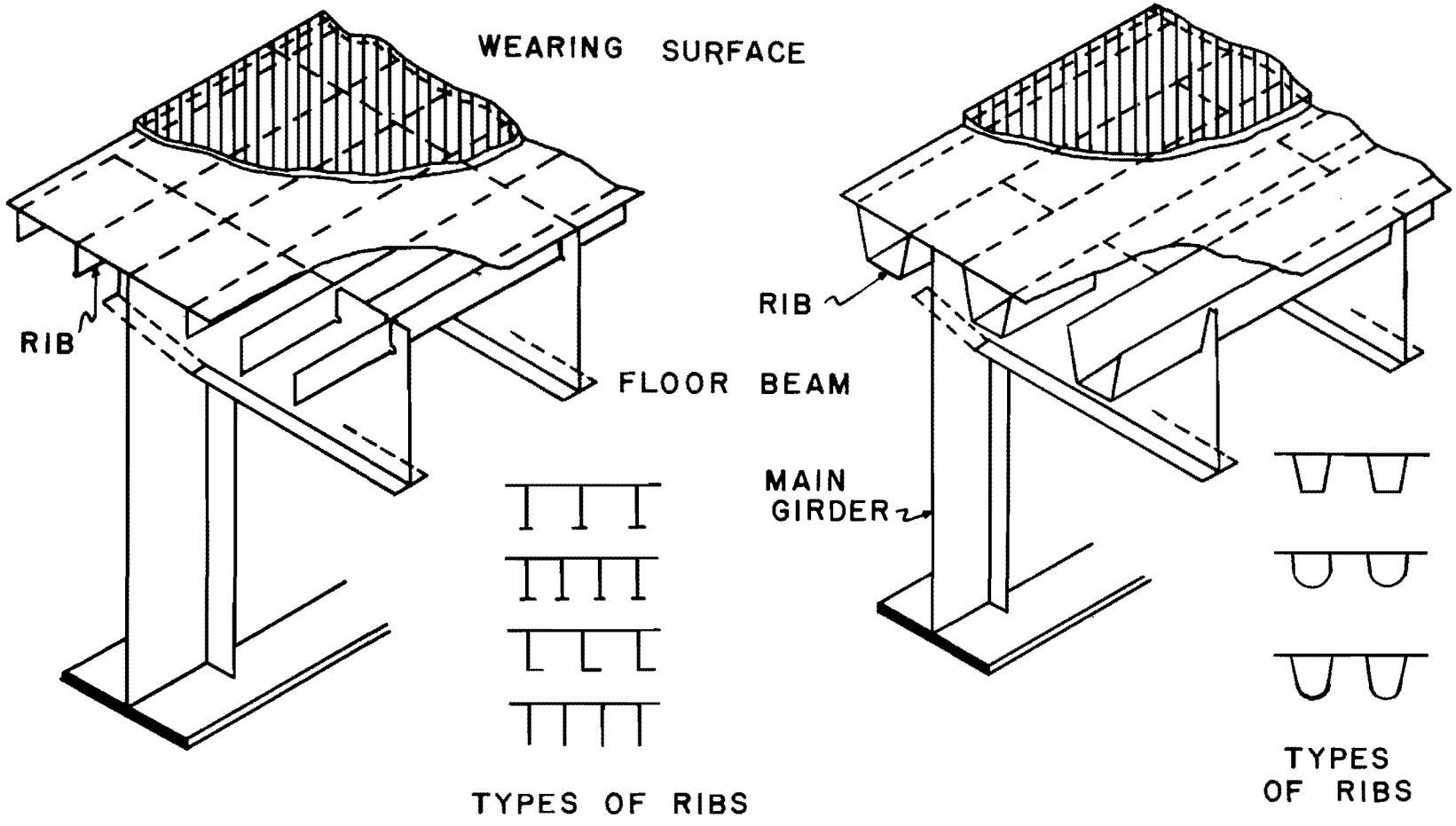

ORTHOTROPIC STEEL DECK PLATE BRIDGES

FIGURE 1.

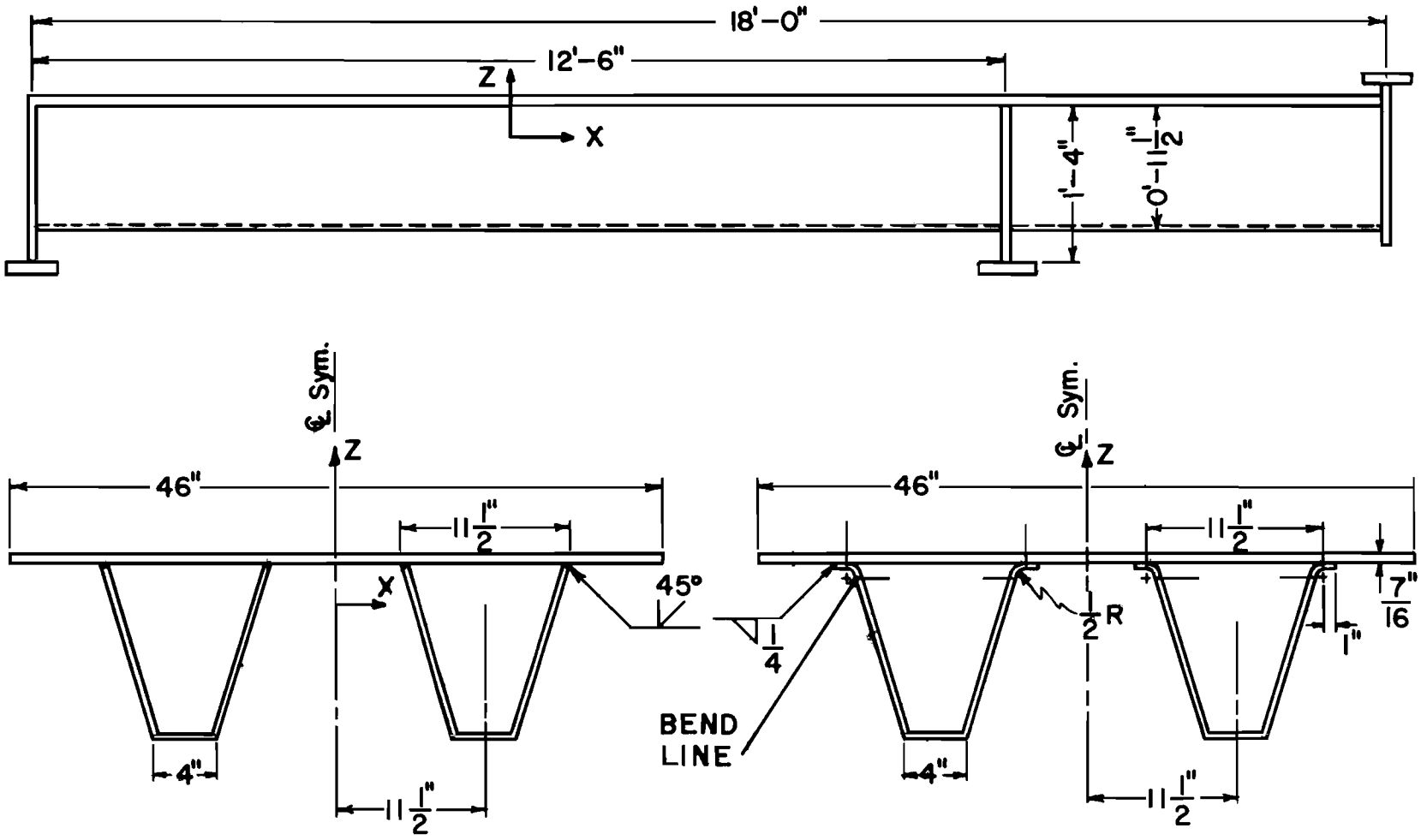

TEST SPECIMEN

FIGURE 2.

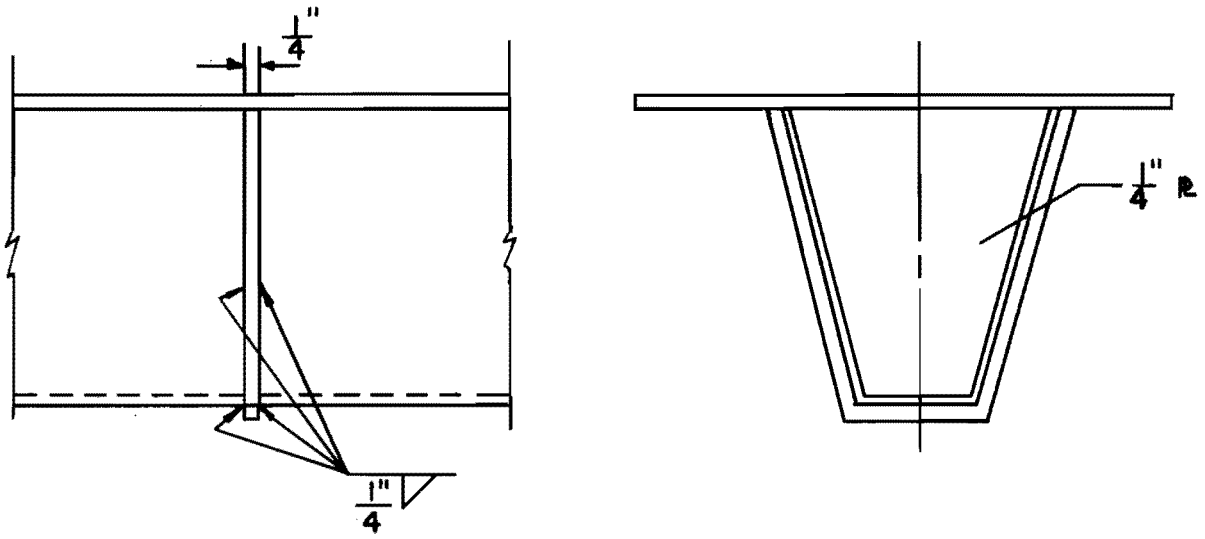

DIAPHRAGM SPLICE

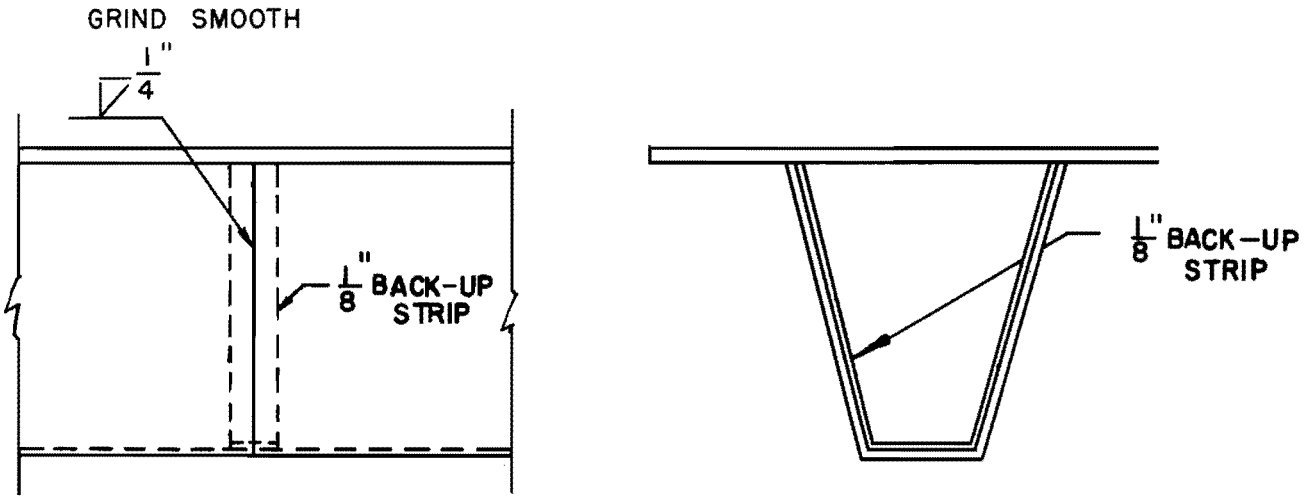

BUTT WELD SPLICE

RIB SPLICES

FIGURE 3.

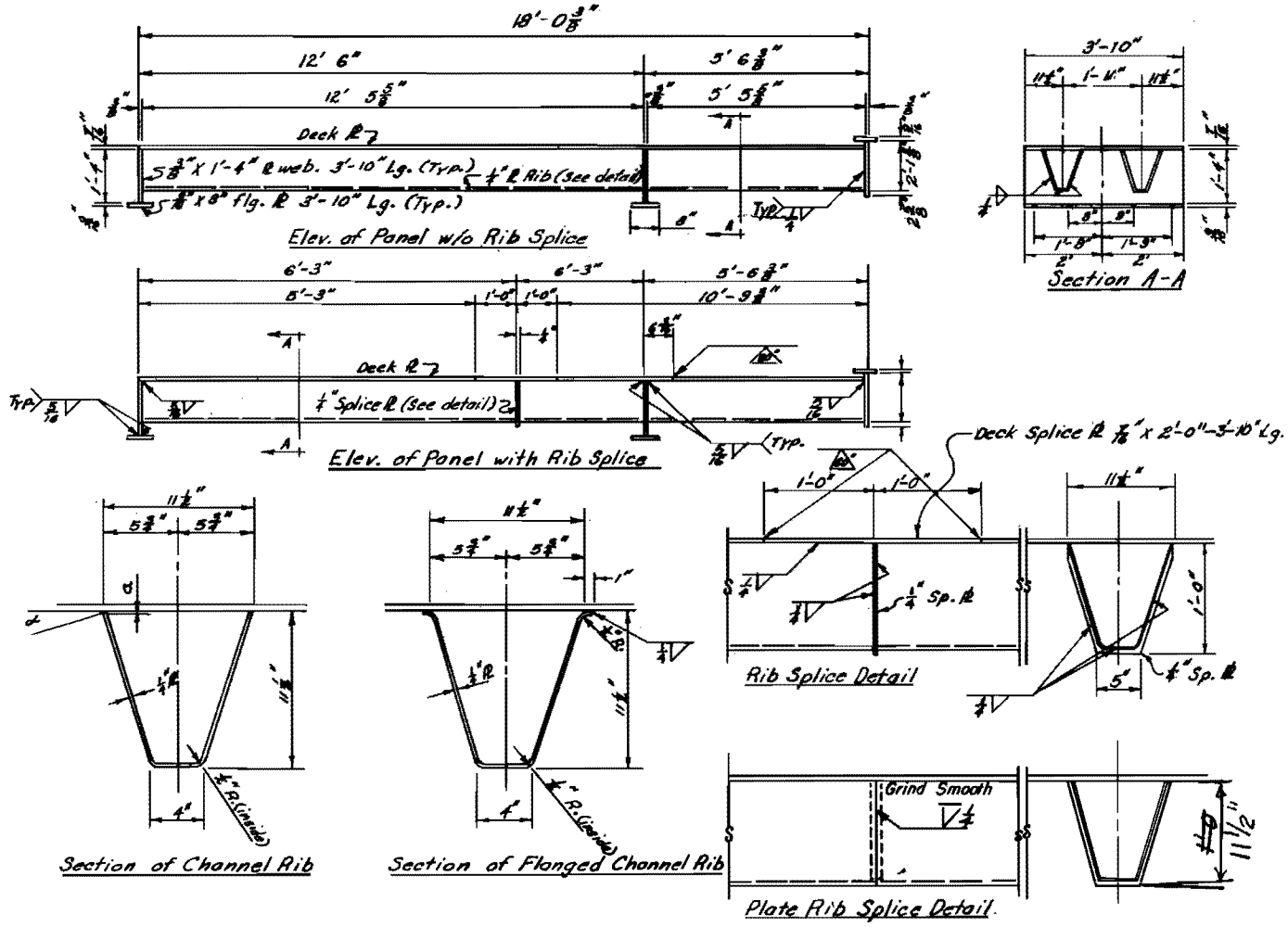

	α	a
Subm Arc	60°	0"
Manual	45°	1/8"

Make 2 panels with channel rib without rib splice.
Make 1 panel with chonnel rib with rib splice.
Make 2 panels with flanged channel ribs without rib splice.
All steel is A 36 steel.

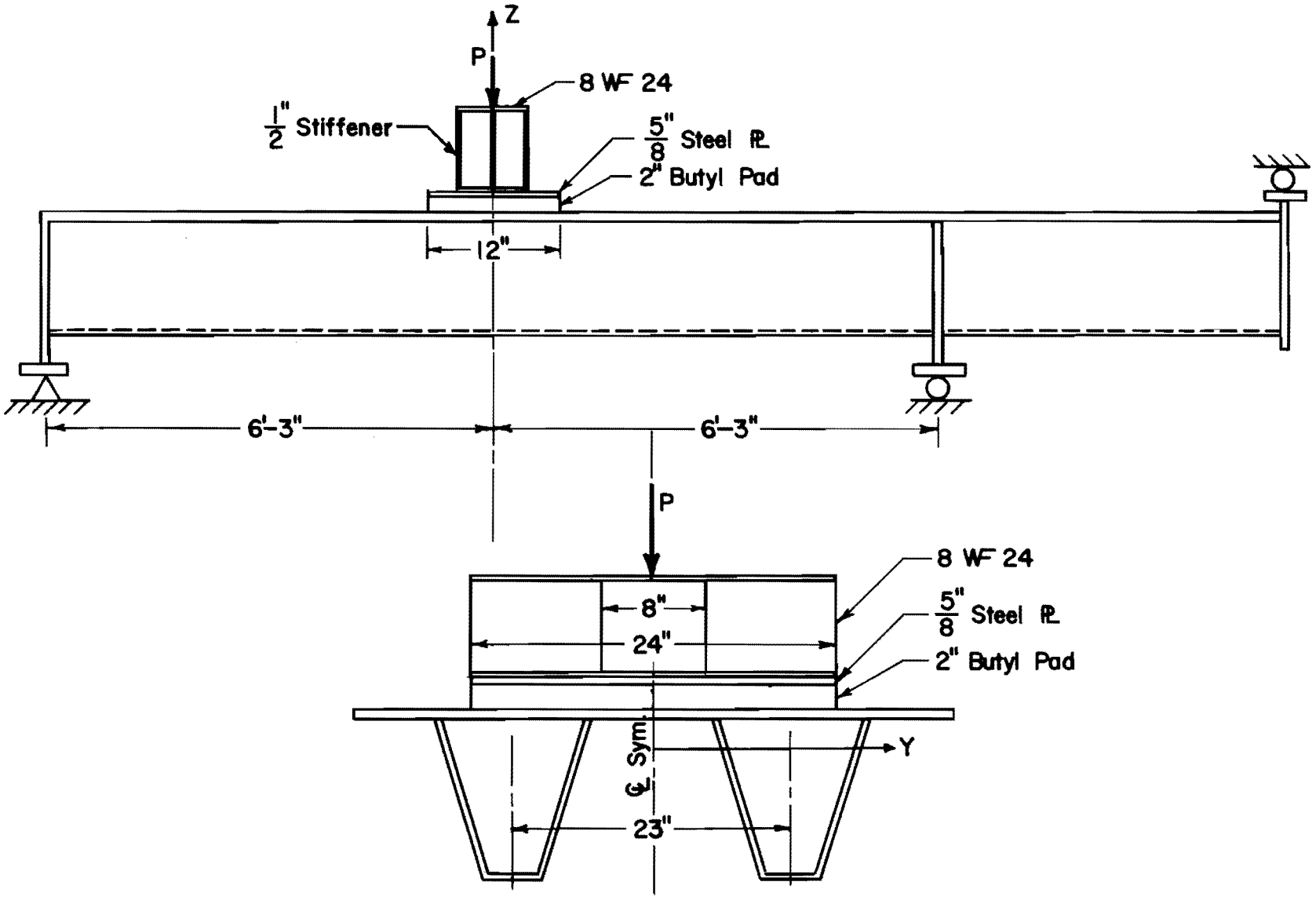

TEST SET UP

FIGURE 5.

TEST SET UP

FIGURE 6.

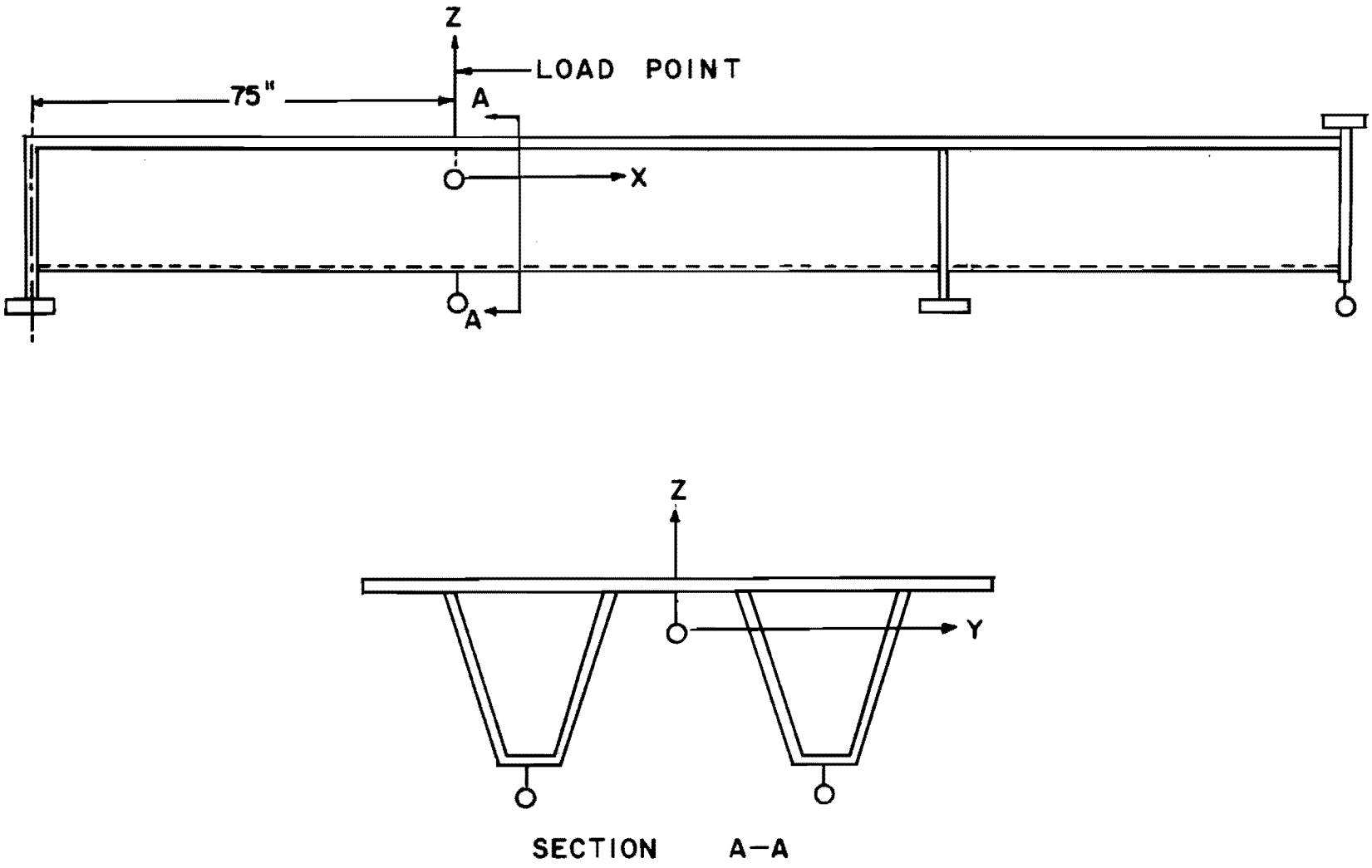

DIAL GAGE LOCATIONS

FIGURE 7.

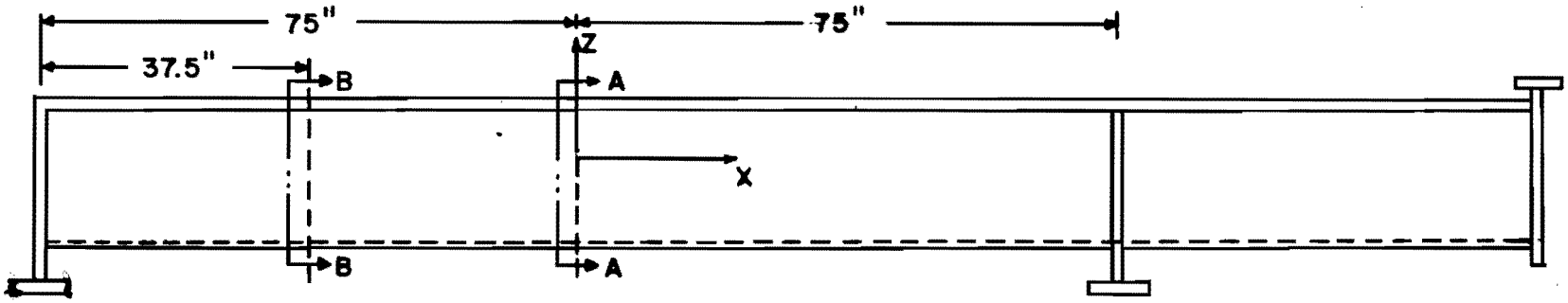

SECTION B – B

ONE-QUARTER POINT

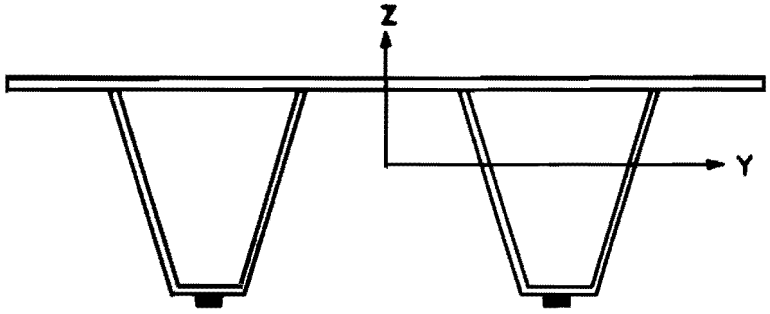

SECTION A – A

LOAD POINT

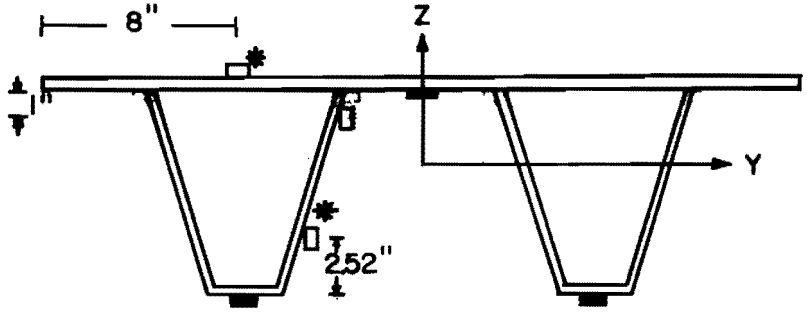

ROSETTE GAUGES ARE INDICATED BY ✱ ALL OTHER GAUGES ARE BIAXIAL

■ ALL SPECIMENS ▭ SPECIMEN 2 AND 3 ONLY

STRAIN GAGE LOCATIONS

FIGURE 8,

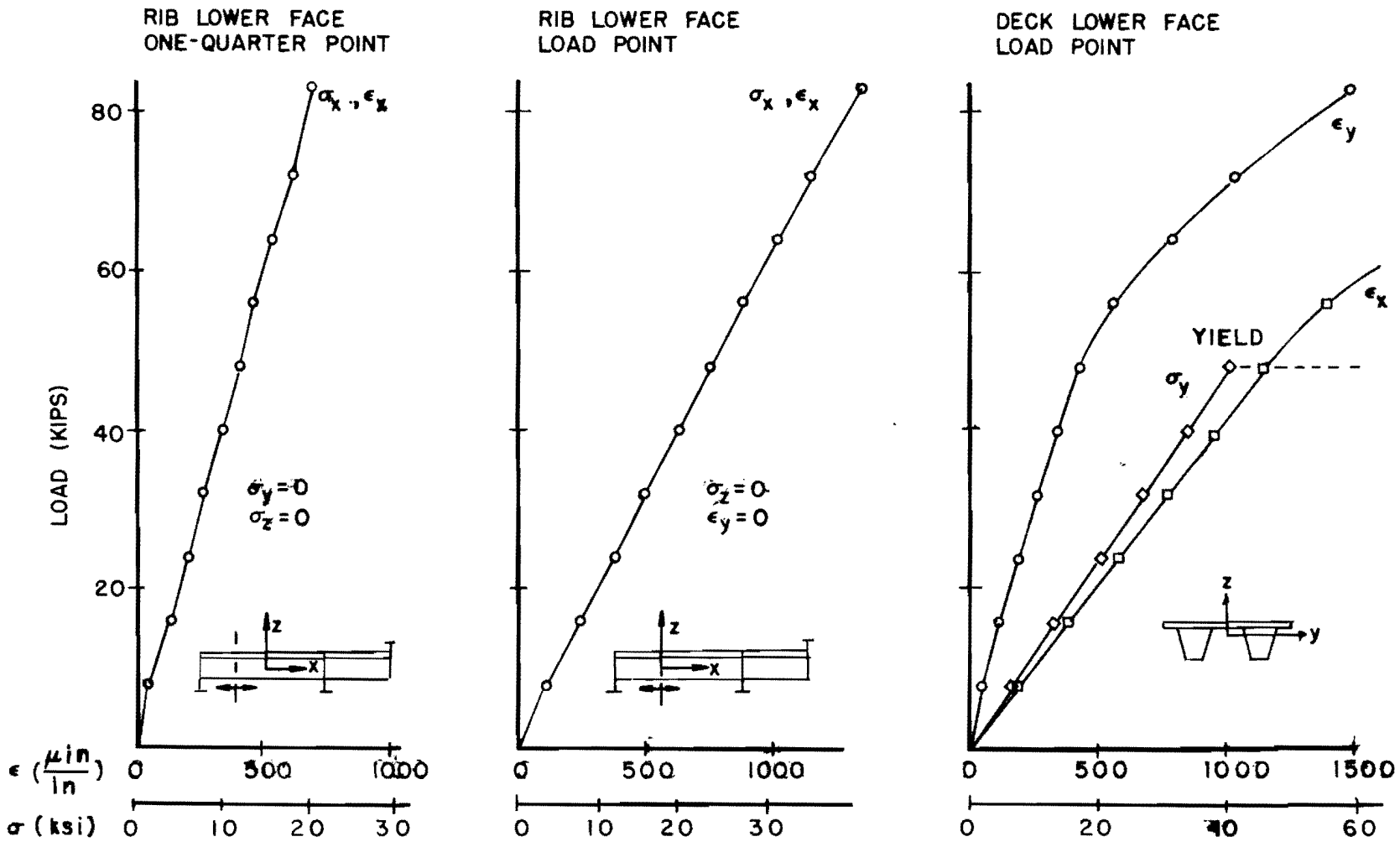

STATIC TEST RESUETS

Specimen 1 (Flanged)

FIGURE 9.

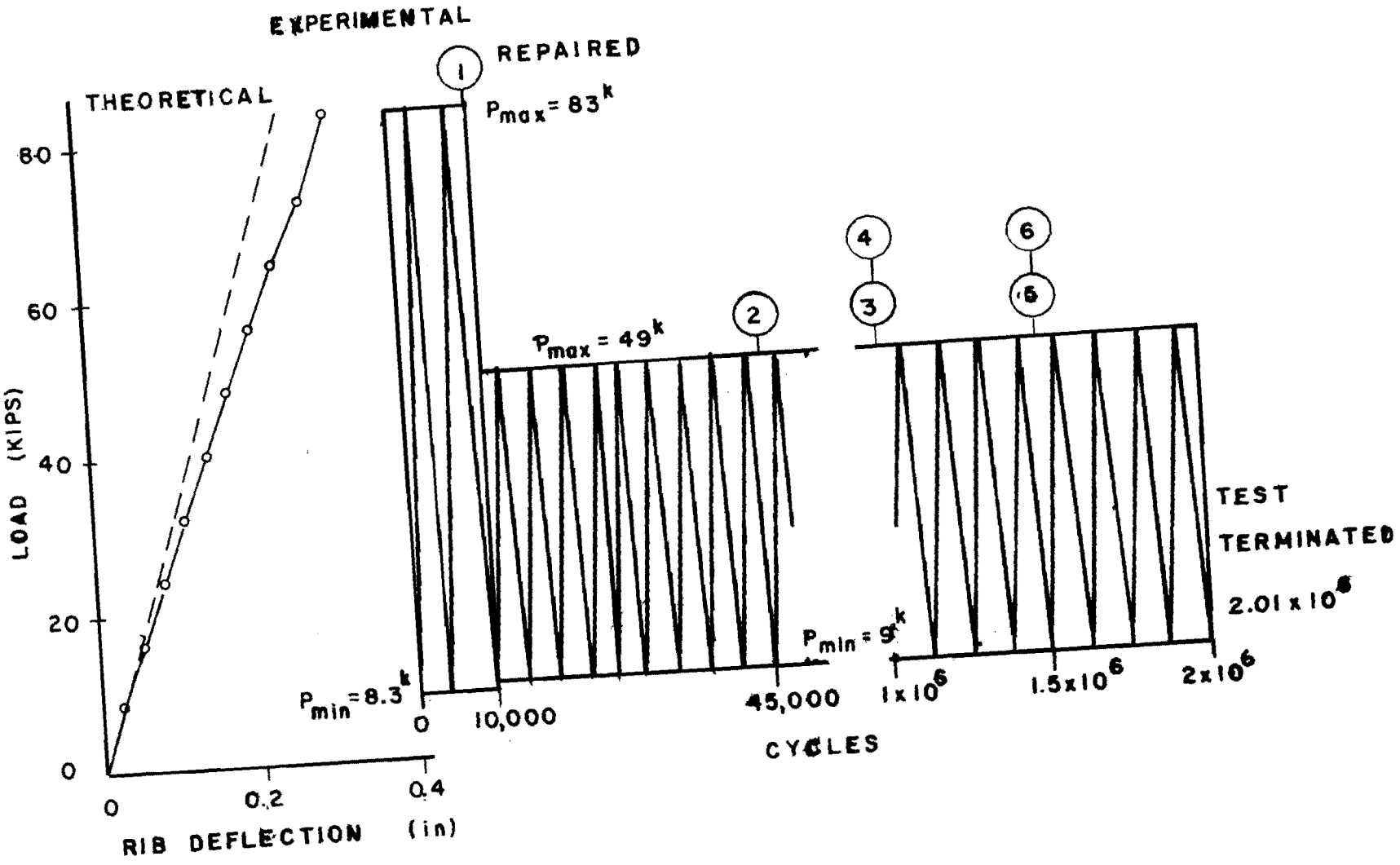

FATIGUE TEST RESULTS
Specimen 1 (Flanged)

FIGURE 10.

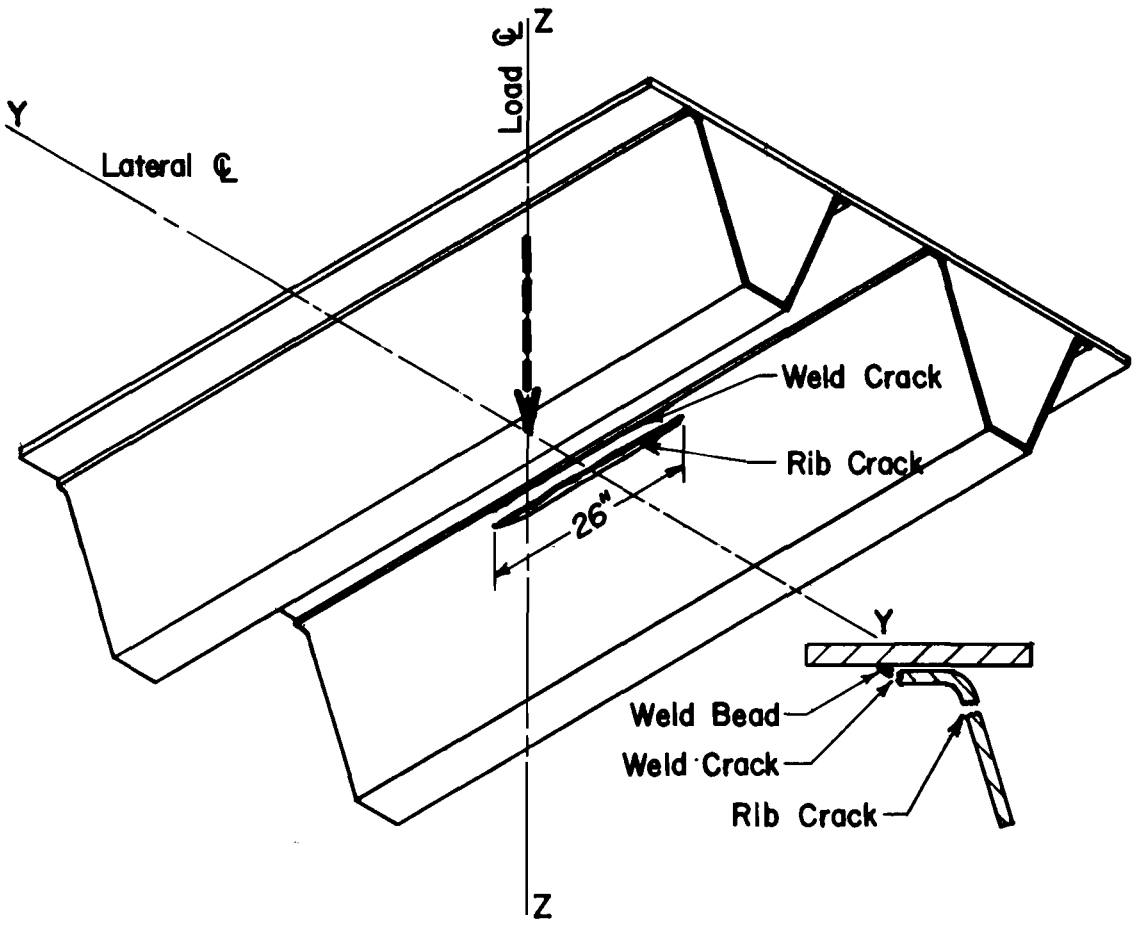

Weld Cracks - Rib to Deck Connection

FIGURE 11.

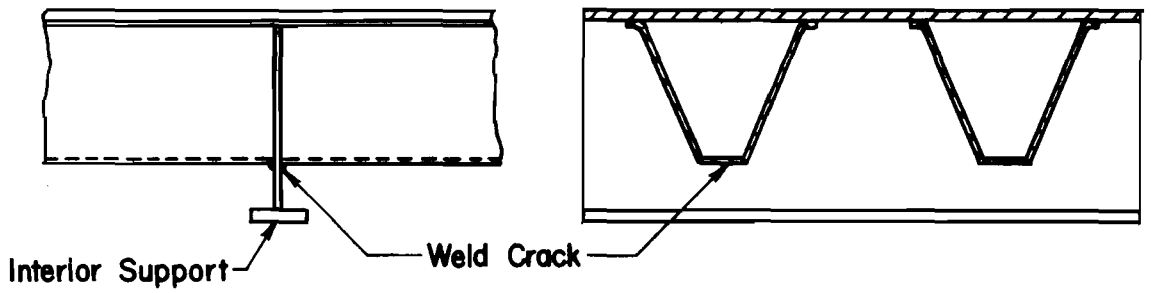

Weld Crack - Lower Face of Rib at Interior Support

FIGURE 12.

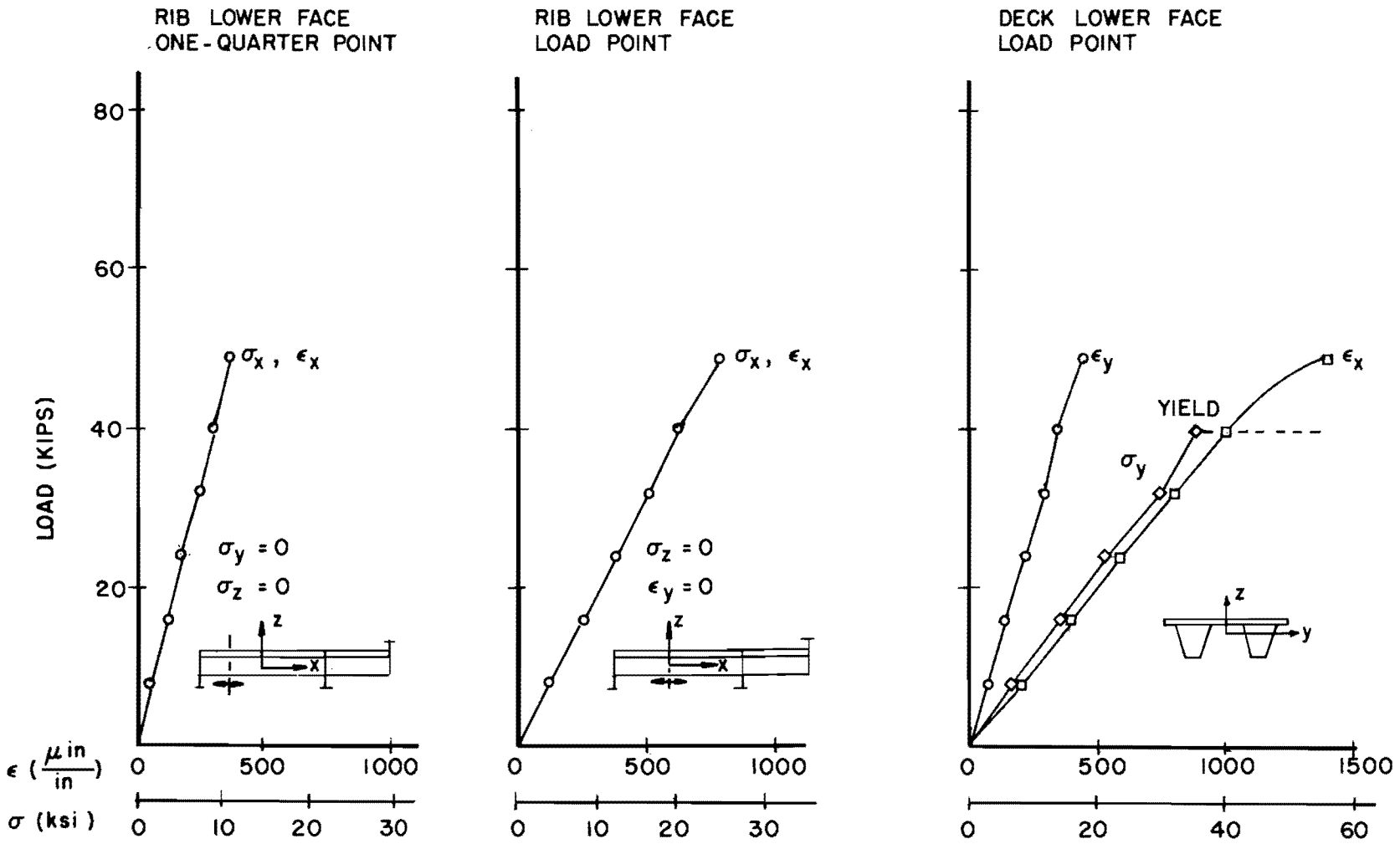

STATIC TEST RESULTS
Specimen 2 (Flanged)

FIGURE 13.

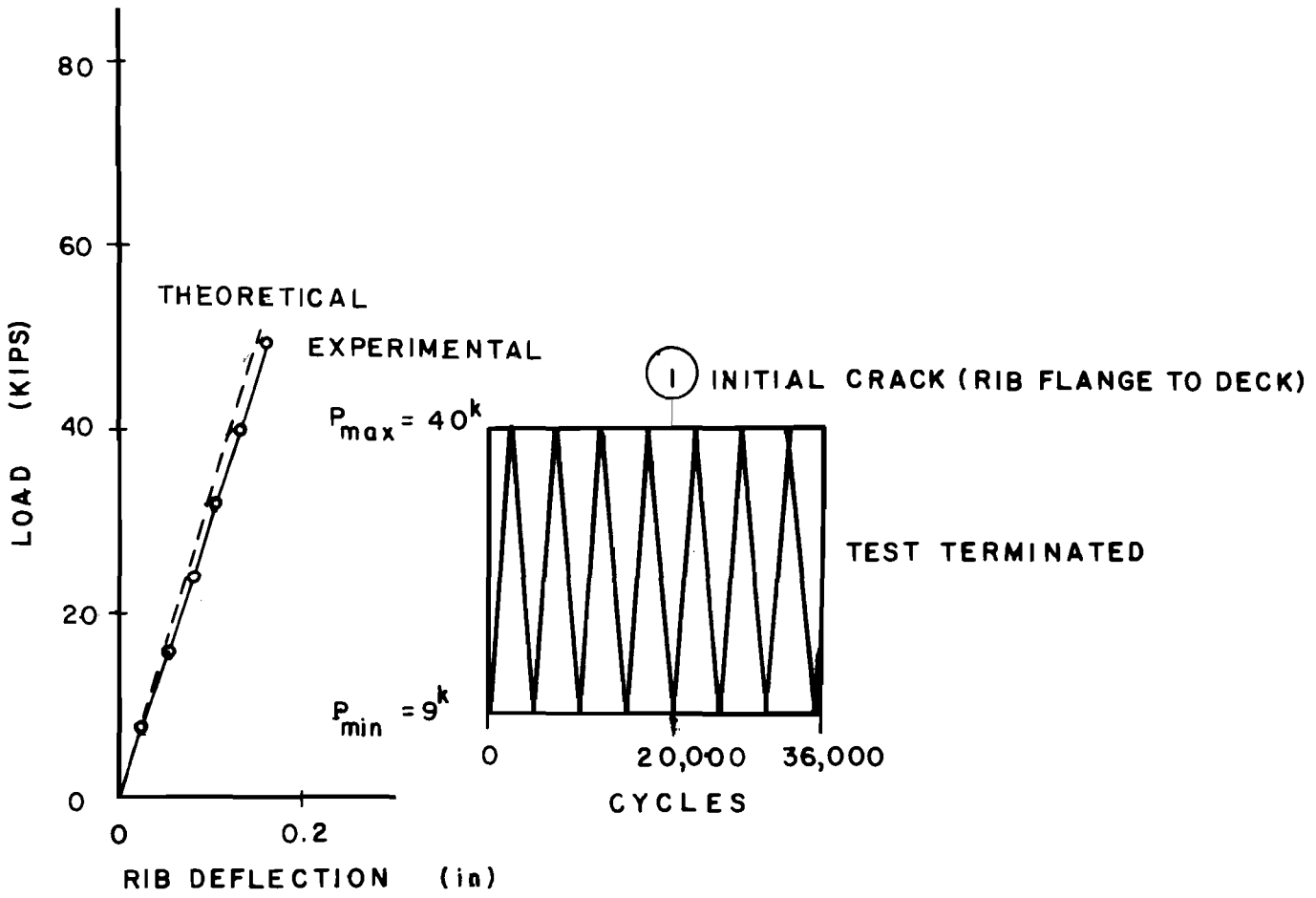

FATIGUE TEST RESULTS
Specimen 2 (Flanged)

FIGURE 14.

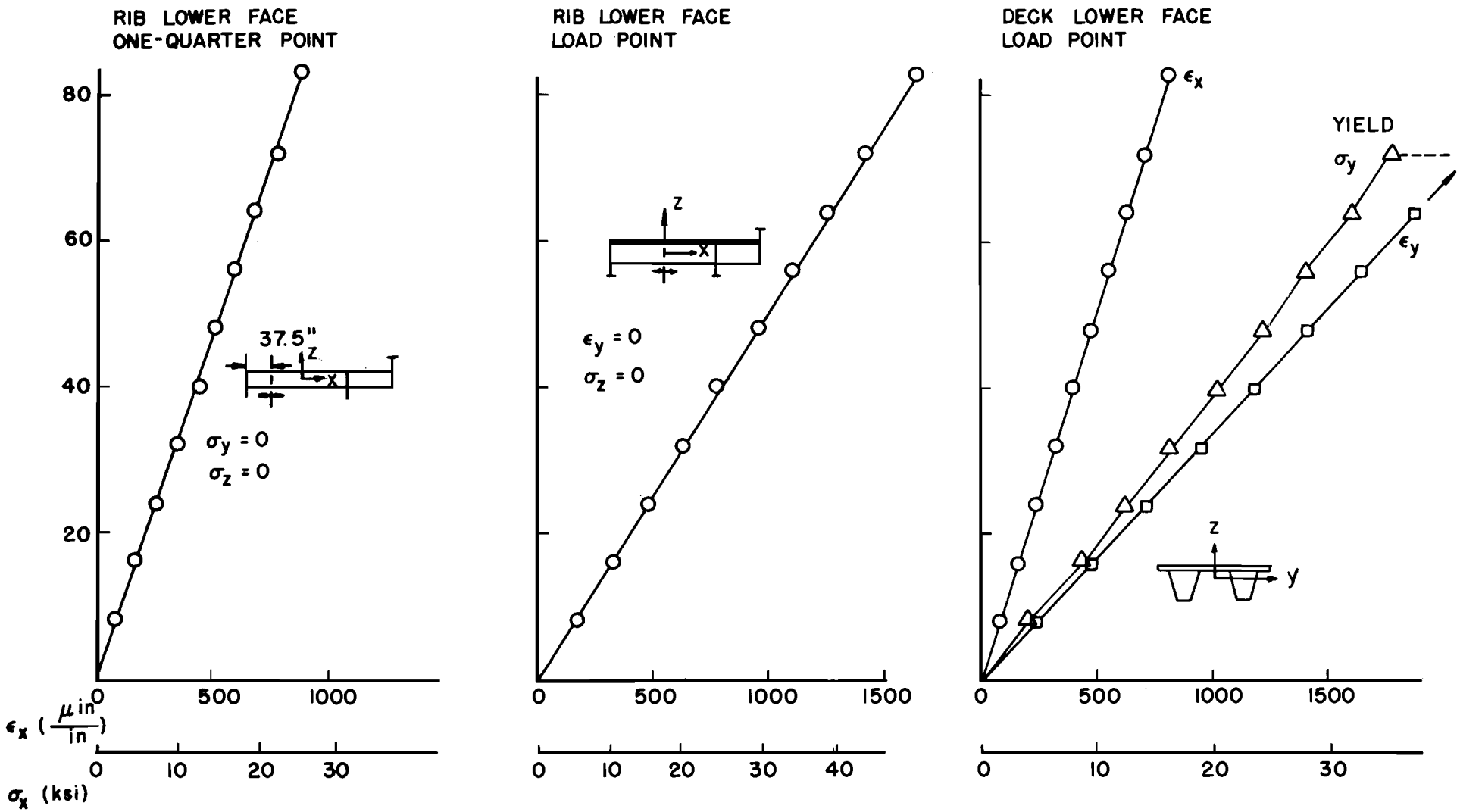

STATIC TEST RESULTS

Specimen 3. (Unflanged)

FIGURE 15.

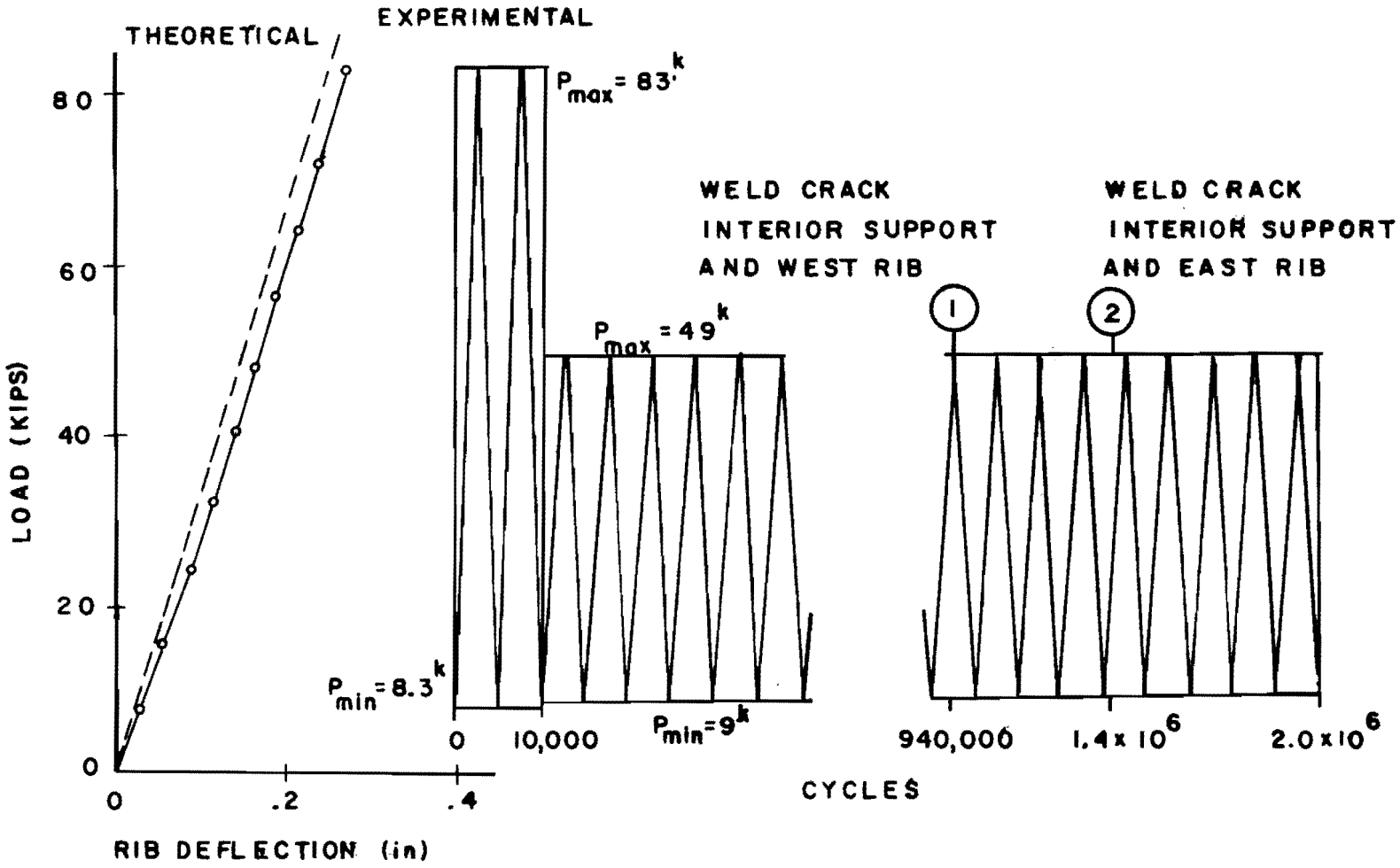

FATIGUE TEST RESULTS
Specimen 3 (Unflanged)

FIGURE 16.

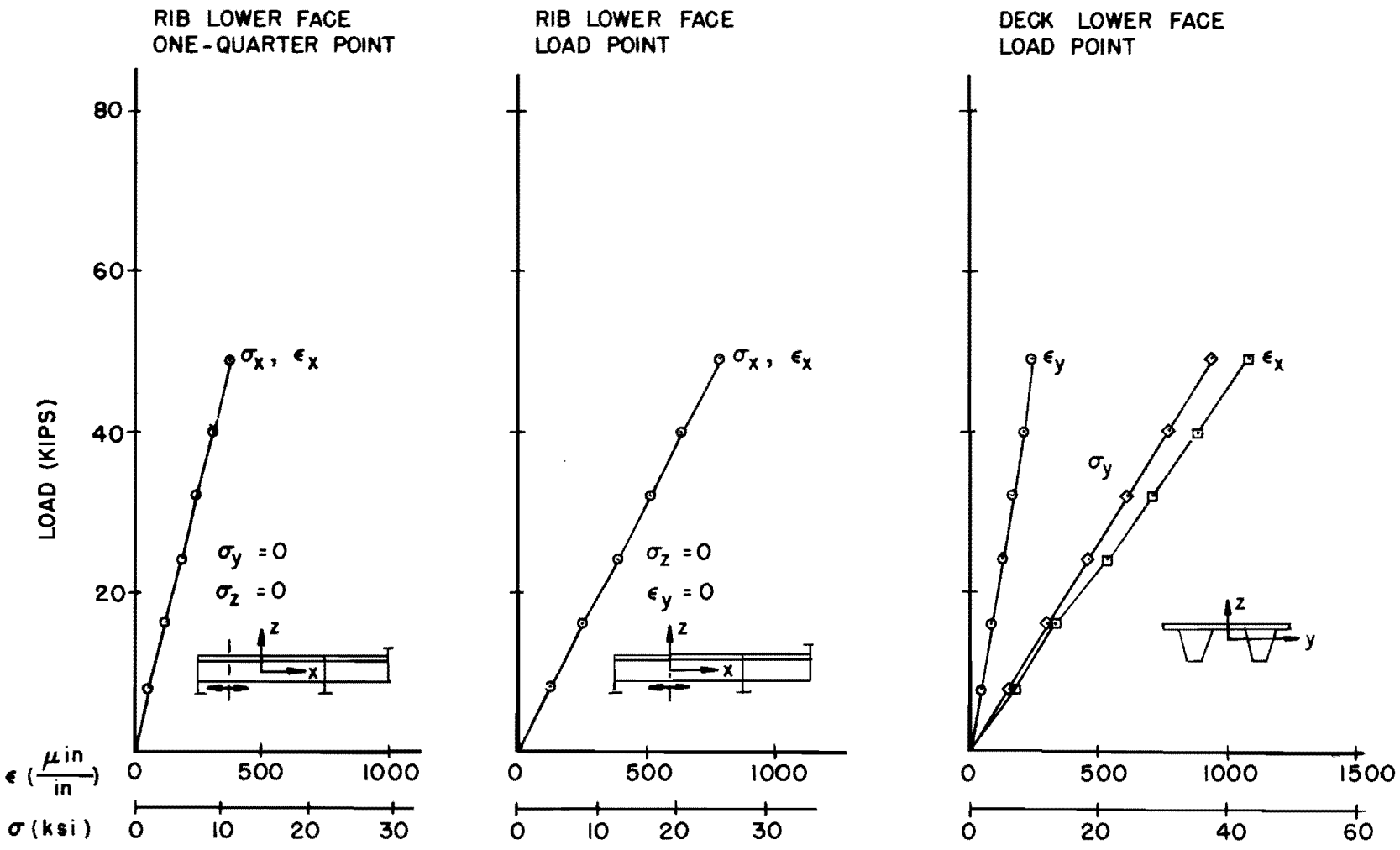

STATIC TEST RESULTS
Specimen 4 (Unflanged)

FIGURE 17.

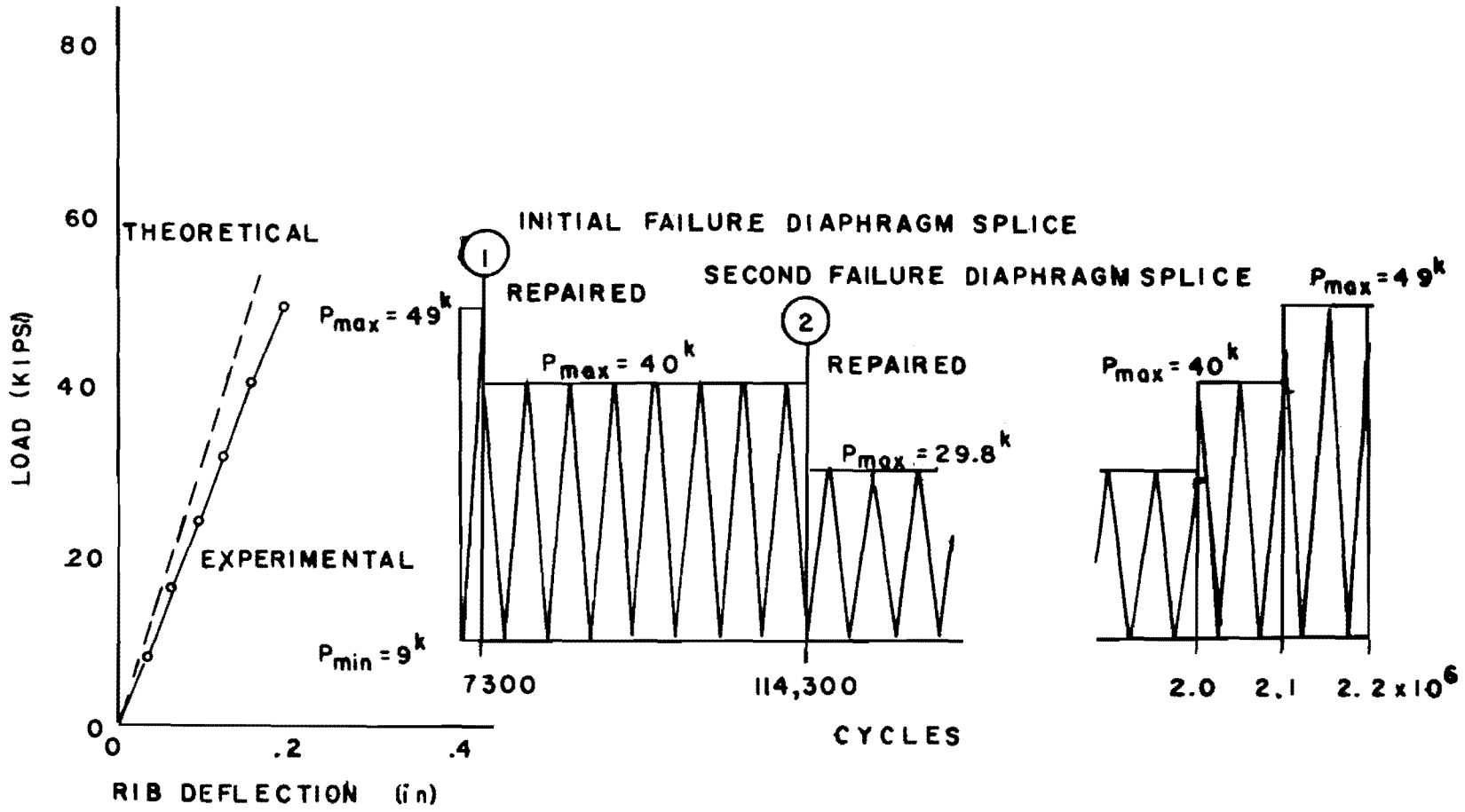

FATIGUE TEST RESULTS
Specimen 4 (Unflanged)

FIGURE 18.

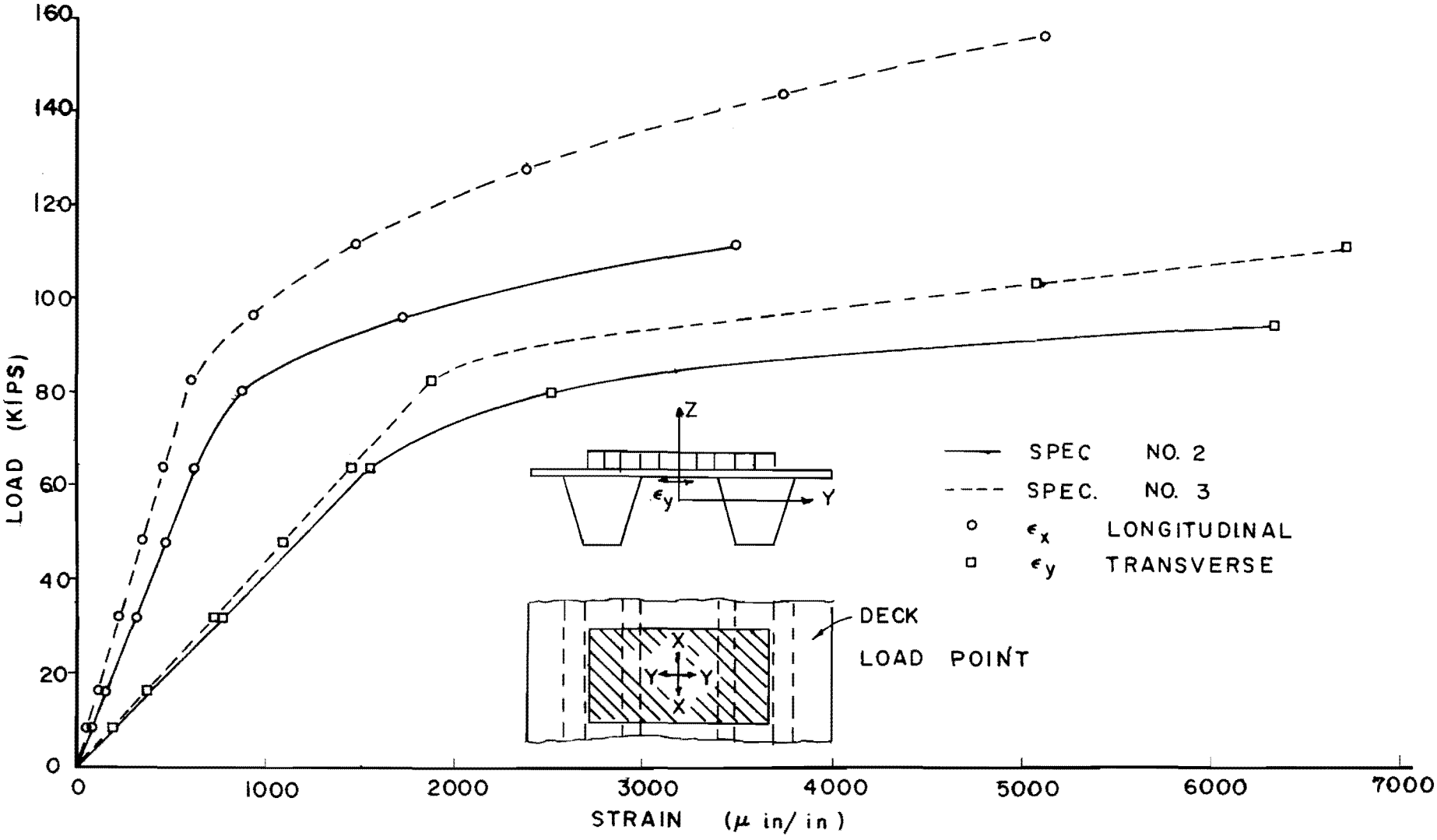

Measured Strains
Ultimate Load Test
Deck Lower Face

FIGURE 19.

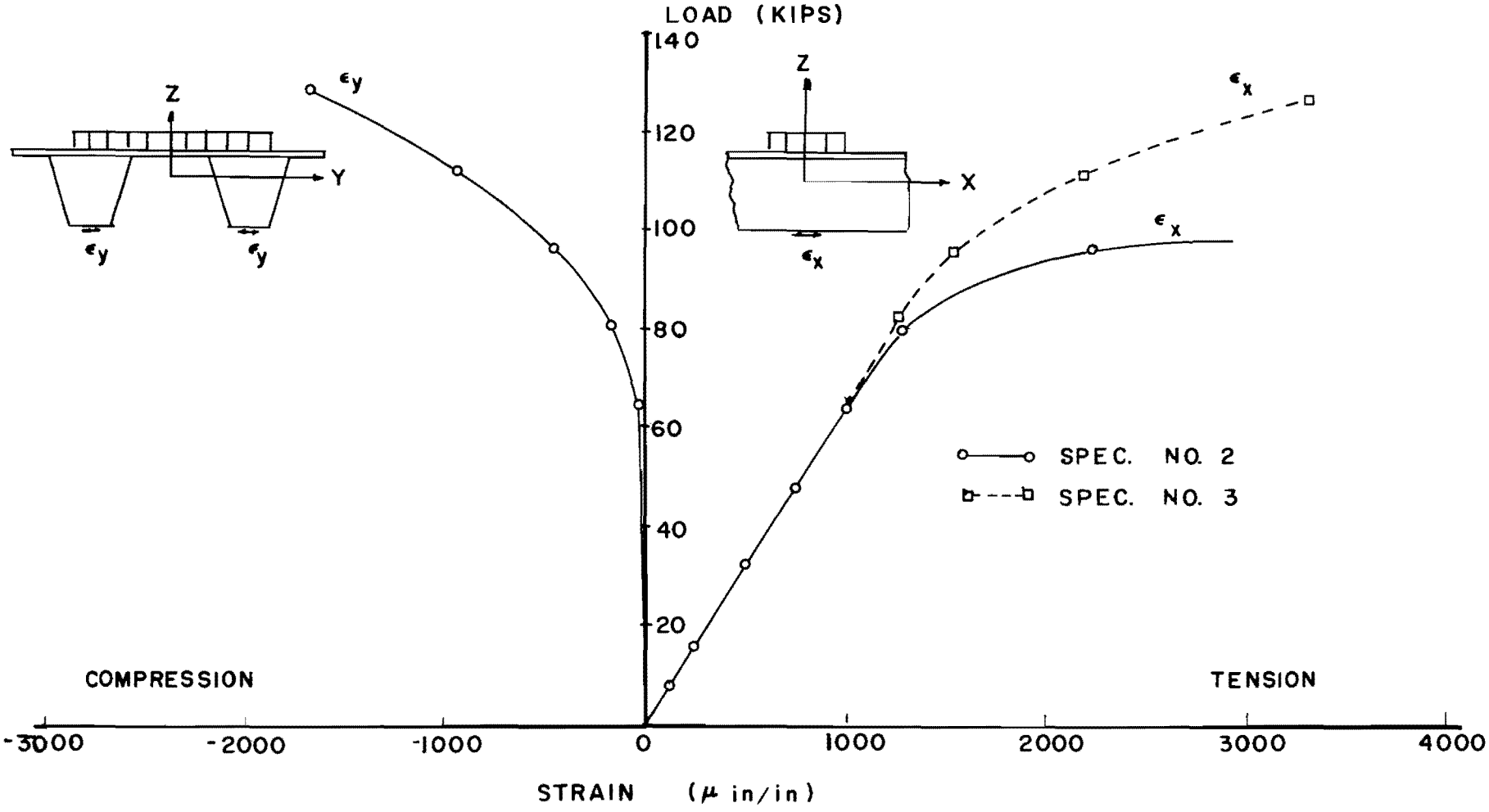

Measured Strains
Ultimate Load Test
Rib Lower Face

FIGURE 20.

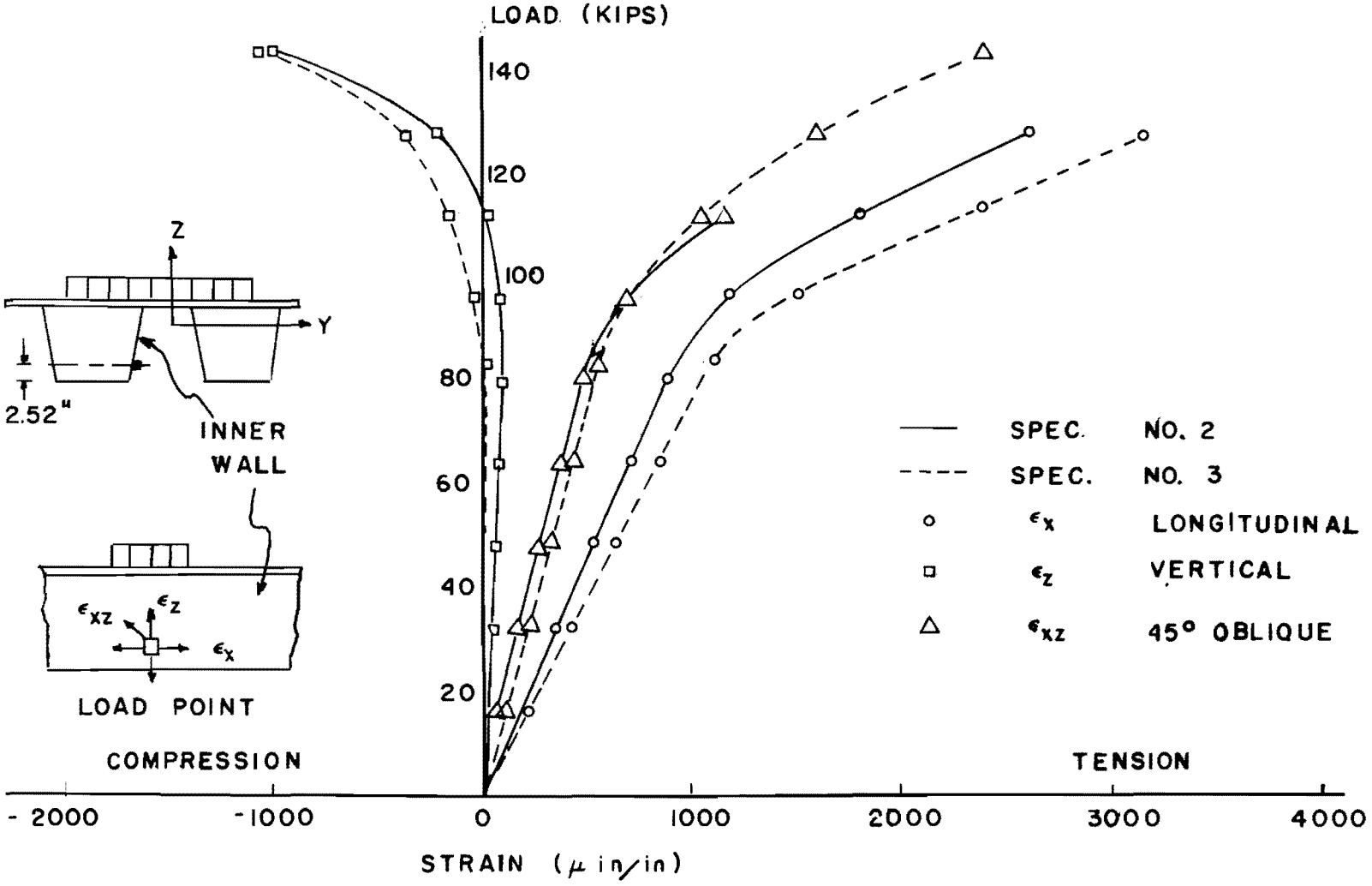

Measured Strains
Ultimate Load Test
Rib Inner Wall - Tension Zone

FIGURE 21.

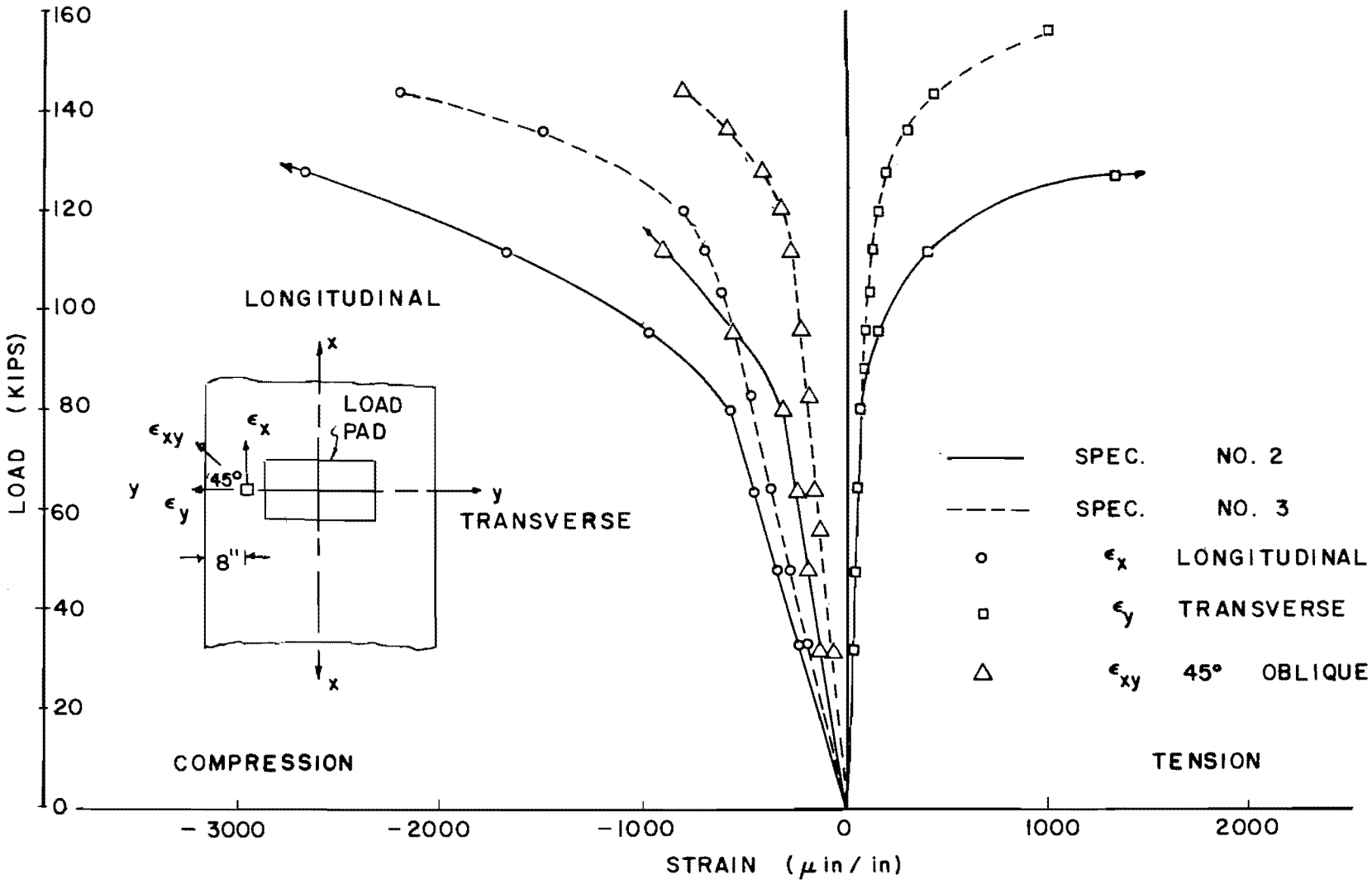

Measured Strains
Ultimate Load Test
Deck Upper Face

FIGURE 22.

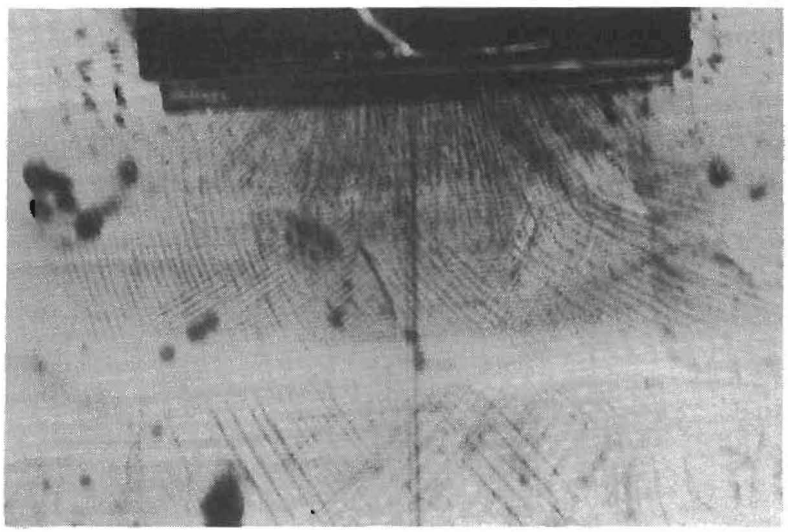

Compression Yielding of Deck

FIGURE 23.

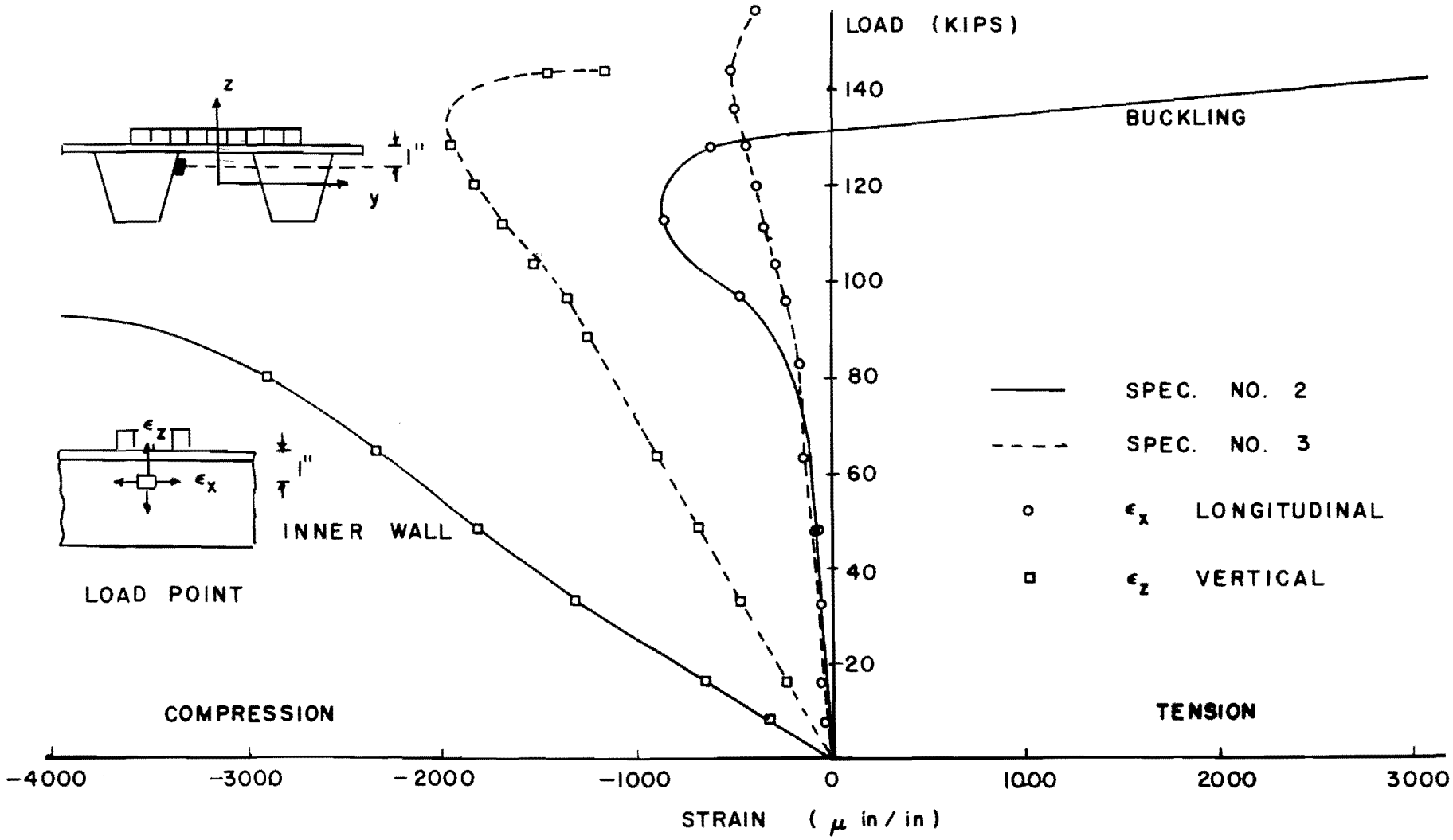

Measured Strains
Ultimate Load Test
Rib Inner Wall - Compression Zone

FIGURE 24.

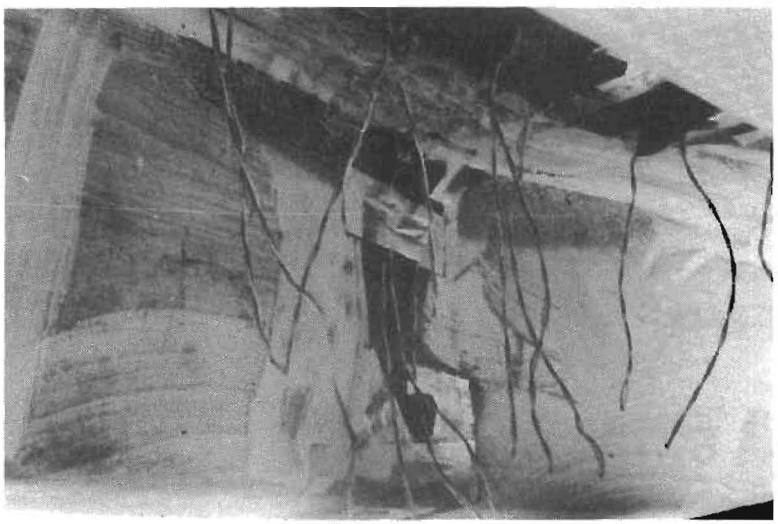

Buckling of Rib Inner Wall
Flanged Specimen

FIGURE 25.

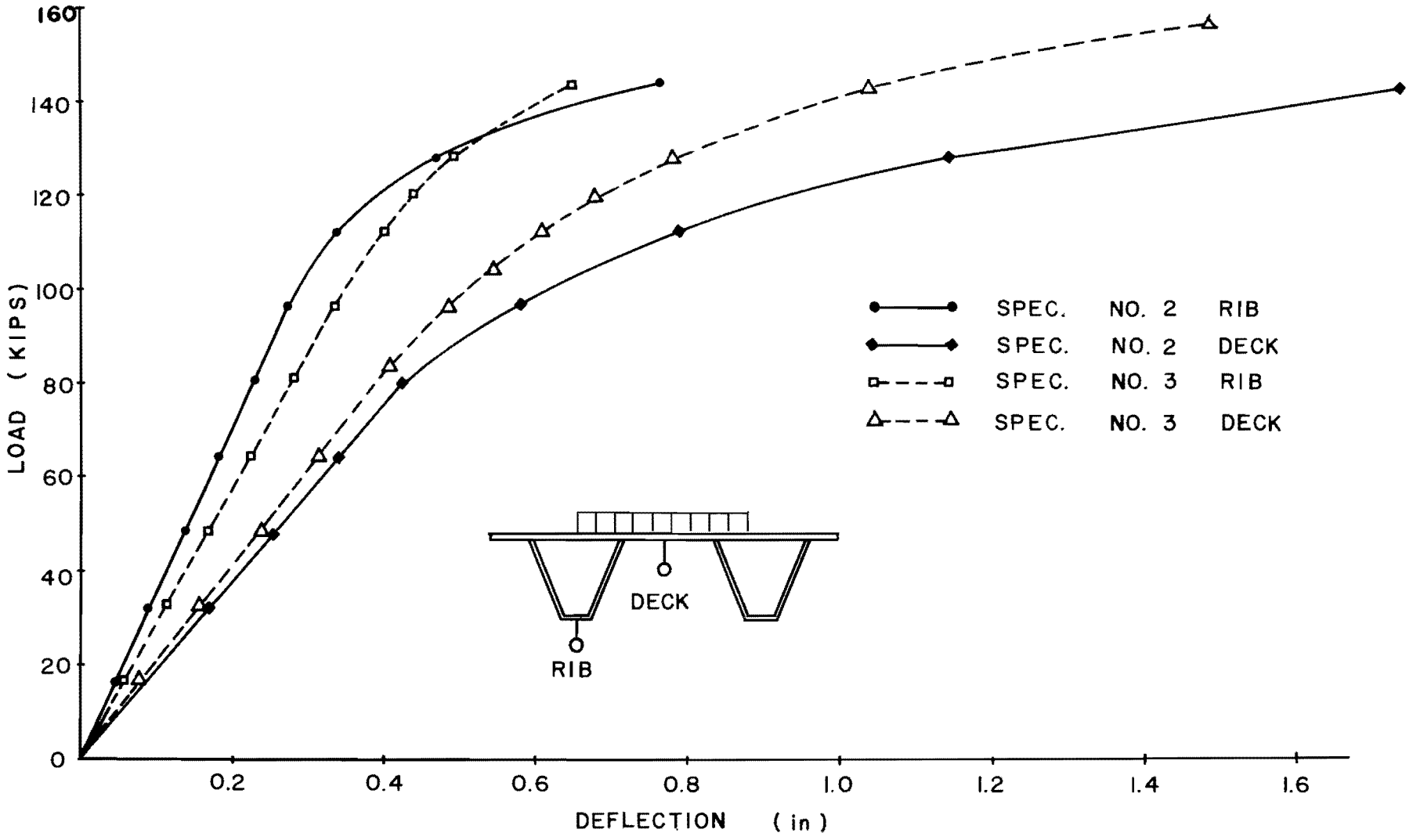

Measured Deflections
Ultimate Load Test
Load Point

FIGURE 26.

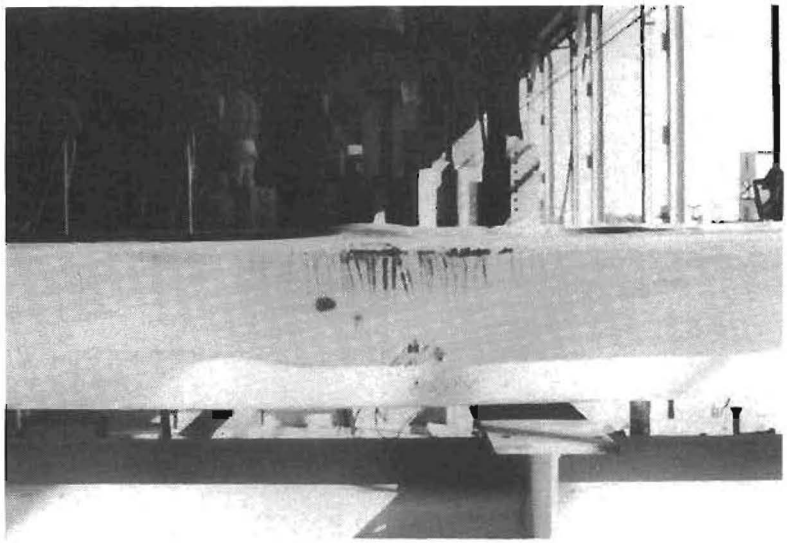

Rib Yielding
Flanged Specimen
FIGURE 27.

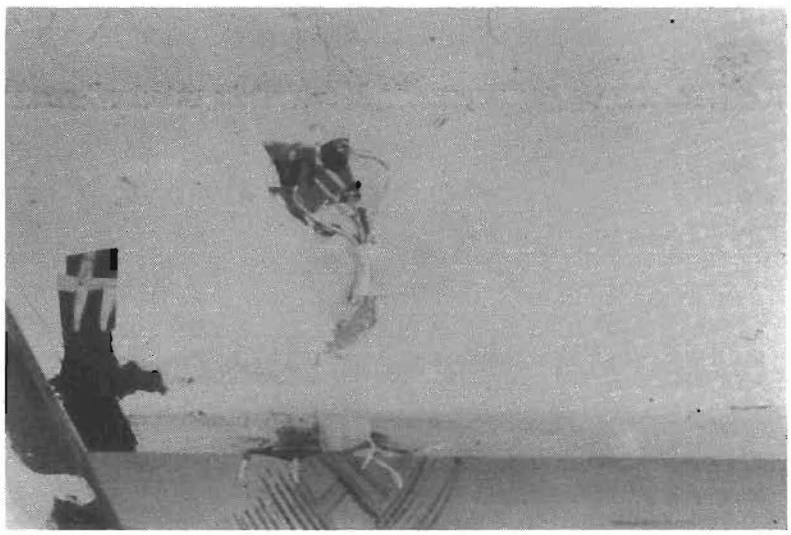

Rib Yielding
Unflanged Specimen
FIGURE 28.

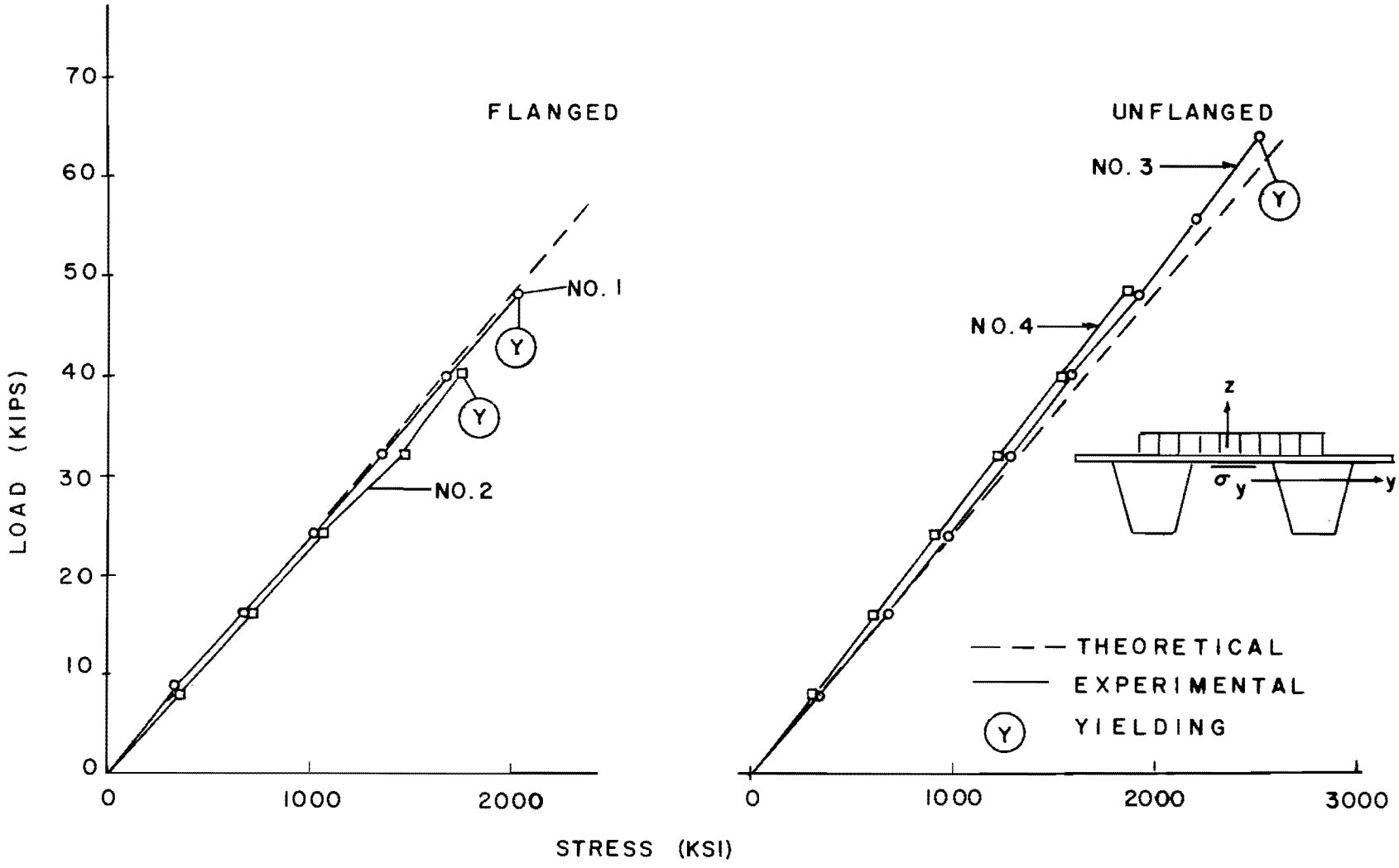

Measured Stresses
Deck Lower Face
Load Point

FIGURE 29.

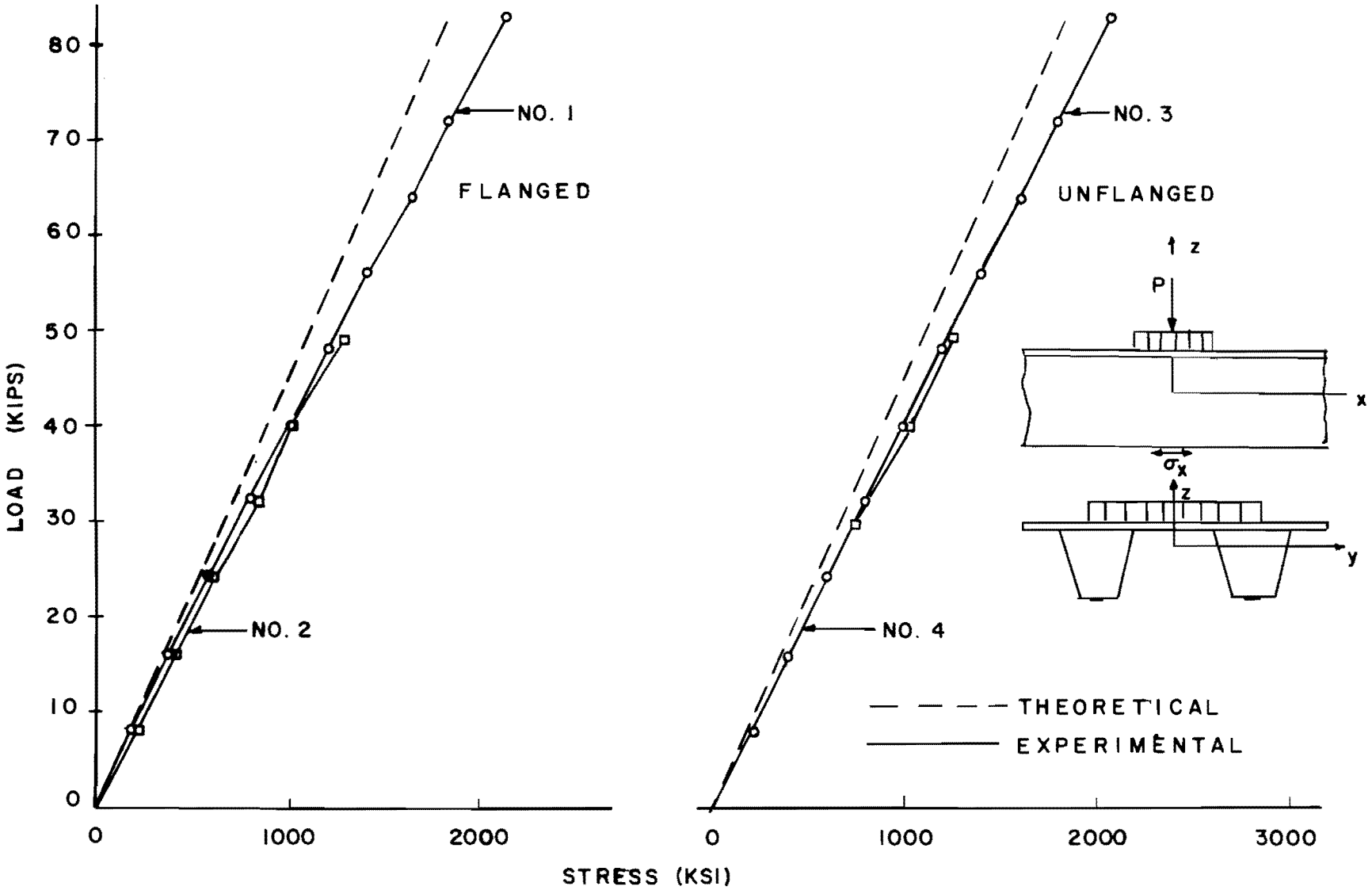

Measured Stresses
Rib Lower Face
Load Point

FIGURE 30.

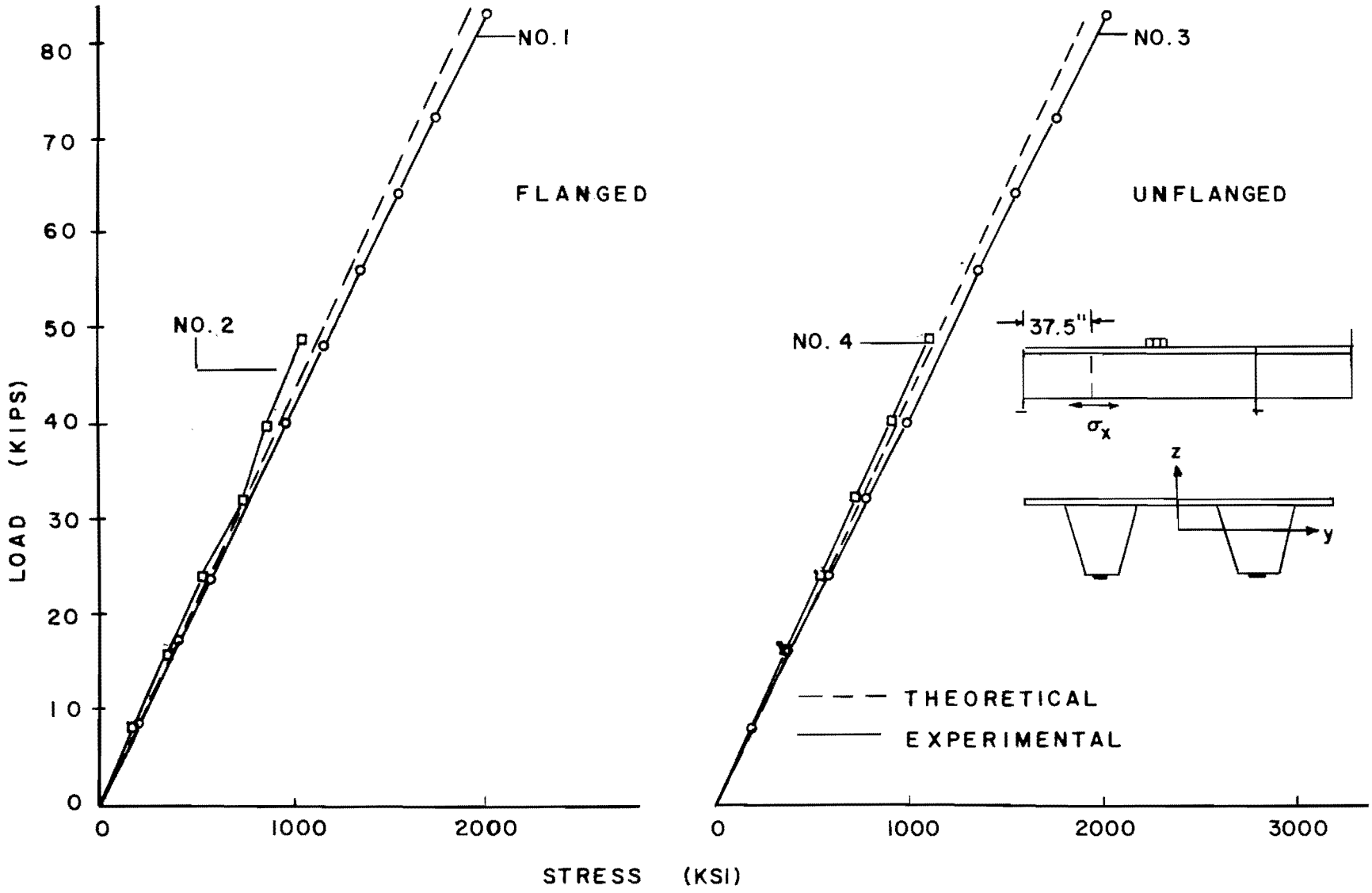

Measured Stresses
Rib Lower Face
One-Quarter Point

FIGURE 31.

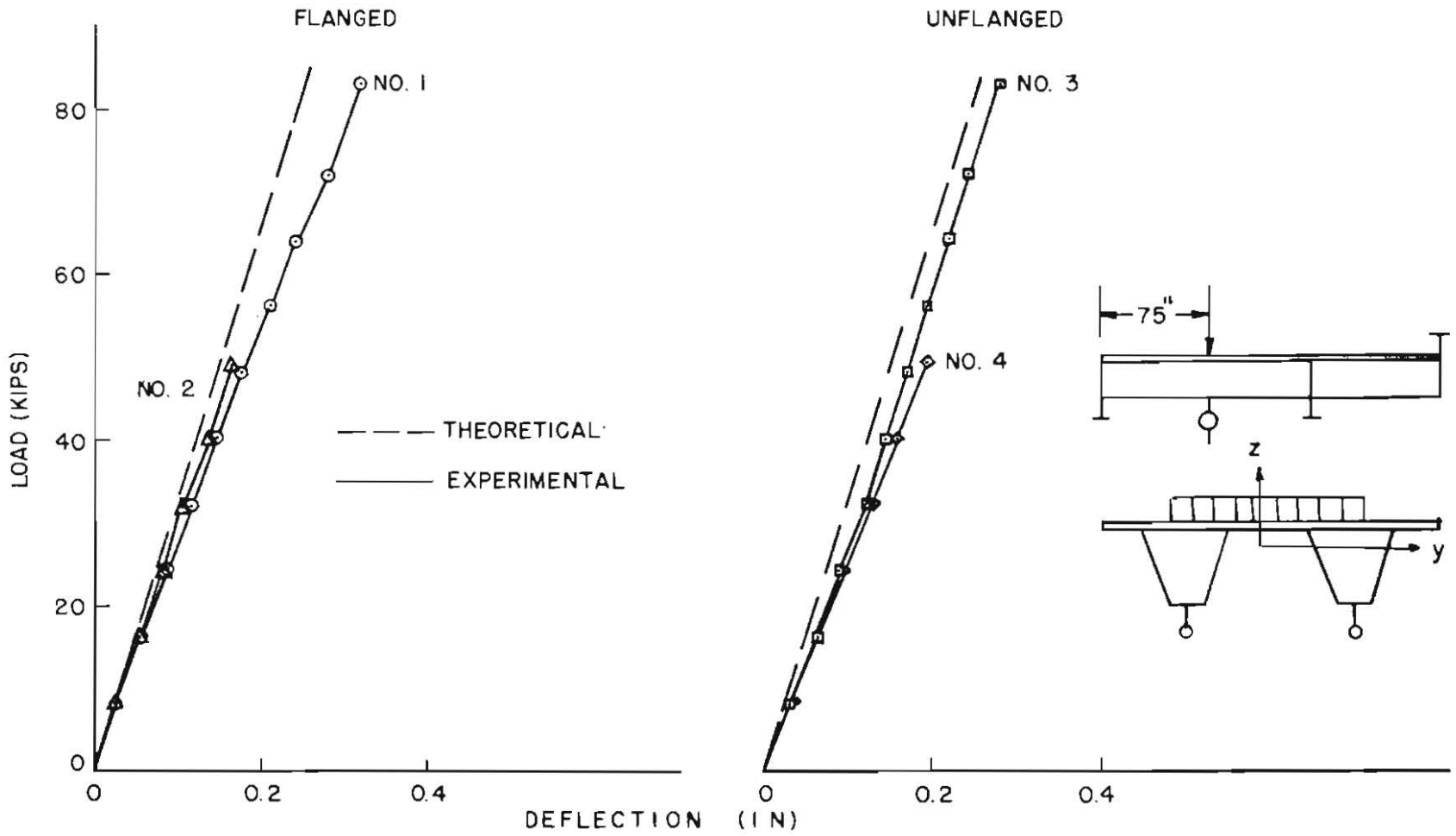

Measured Deflections
Rib Lower Face
Load Point

FIGURE 32.

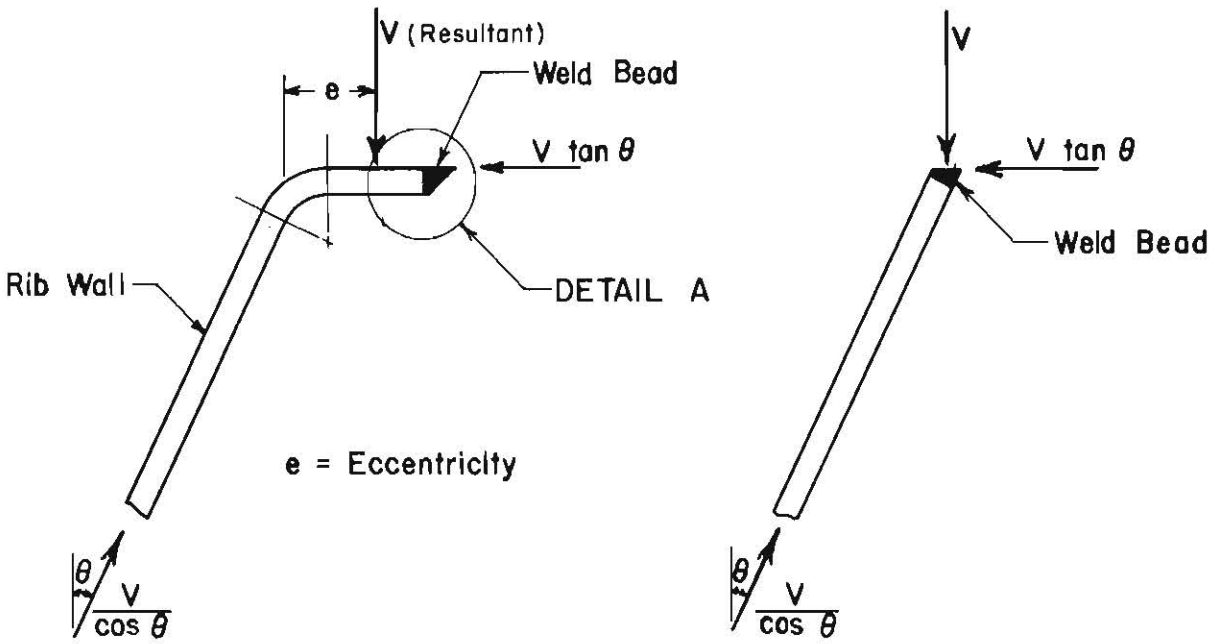

FLANGED

UNFLANGED

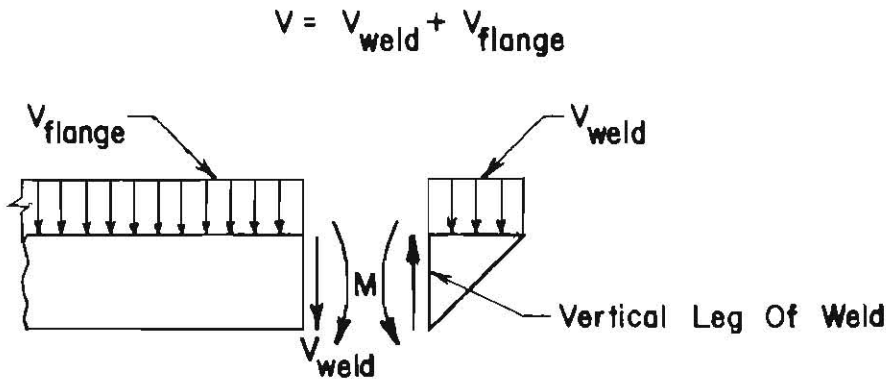

DETAIL A

Load Equilibrium -- Rib to Deck Connection

FIGURE 33.

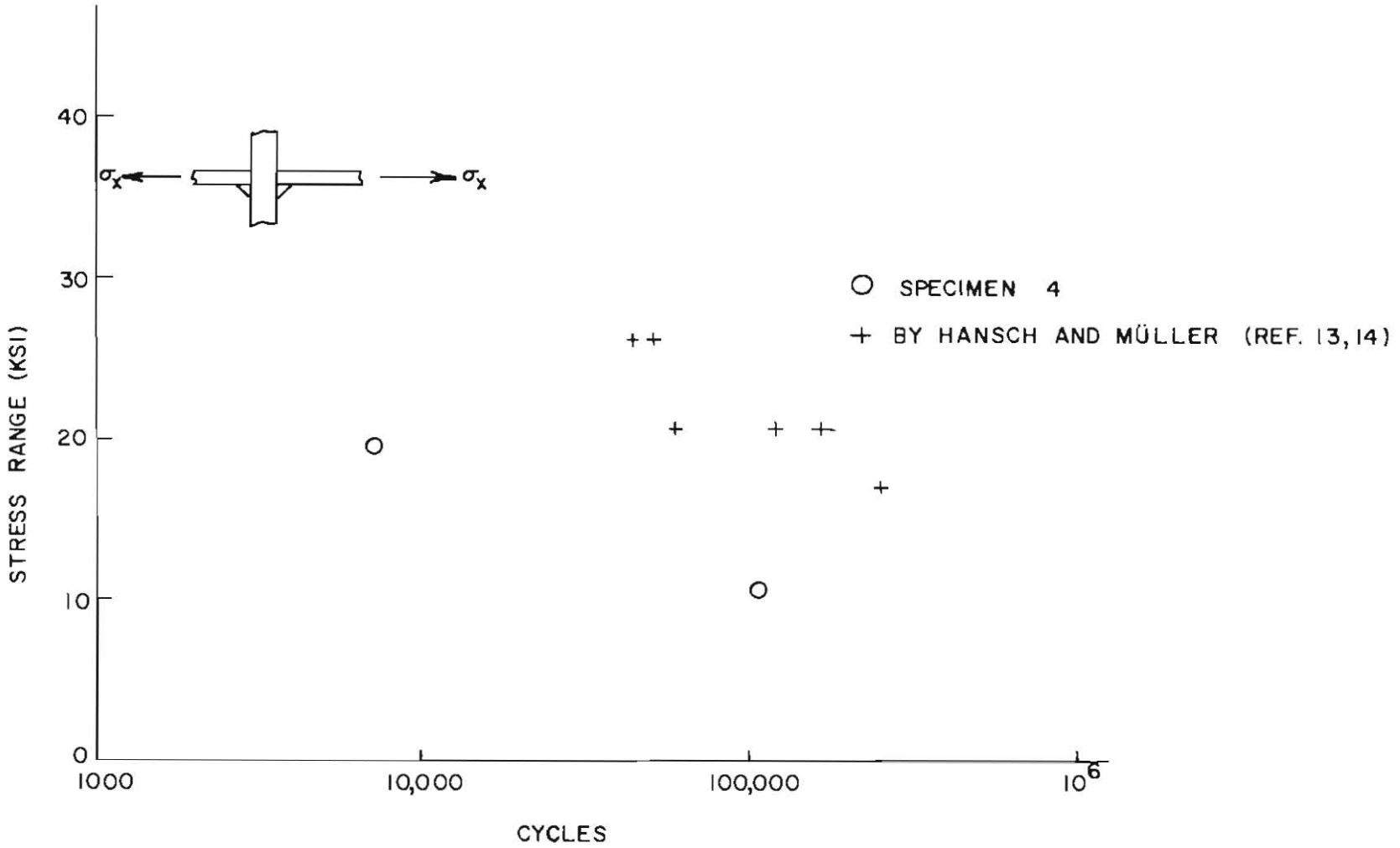

Fatigue Test Results
Diaphragm Plate Rib Splice

FIGURE 34.

APPENDIX I

Nomenclature

A_s	Shear area	in^2
c	Distance from neutral axis to point at which flexural stress is calculated	in
E	Modulus of elasticity	psi
G	Shear modulus of elasticity	psi
I	Moment of inertia, total section	in^4
Ip	Moment of inertia, deck plate	in^4
J	Rib Torsional stiffness	in^4
L	Length of long span	in
lp	Clear length of deck between ribs	in
M	Moment	in-kip
M_b	Moment at interior support	in-kip
M_{cl}	Moment at center line long span (load point)	in-kip
M_d	Total deck plate moment	in-kip
M_{max}	Maximum moment--long span	in-kip
M_p	Moment produced by applied load	in-kip
$M_{p'}$	Moment produced by deflection of overhang support	in-kip
$M_{1/4}$	Moment at one-quarter point long span	in-kip
M_ϕ	Deck moment produced by rib rotation	in-kip
P	Applied load	kips
P'	Dummy load applied at overhang support	kips
R_a	Vertical Reaction at fixed shoe support	kips
R_b	Vertical reaction at interior support	kips
R_c	Vertical reaction at overhang support	kips

T	Torque on ribs	in-kips
V	Shear	kips
v	Shear produced by dummy load	kips
w	Load distribution under load pad	kip/in
y	Total rib deflection at load point	in
y_c	Rib flexural deflection due to continuity moments and overhang deflection	in
y_f	Rib flexural deflection at load point	in
y_s	Rib flexural deflection at load point due to simple beam loads	in
y_{sh}	Rib shear deflection at load point	in
Δ	Deflection at overhang	in
ϵ	Strain	in/in
λ	Coefficient for shear deflections	
μ	Poisson's ratio	
σ	Stress	ksi
ϕ	Twist angel of rib of load point	radians
ψ	Plate factor	

Subscripts

flg	Flanged specimen
unf	Unflanged specimen
x, y, z	Cartesian co-ordinates with origin on neutral axis at load point (Fig. 2).

APPENDIX II

Flexural Stresses and Deflections

Theoretical static flexural stresses and deflections are calculated and presented in this section. Stresses were calculated on the lower faces of the ribs at the load point and at the one-quarter point. Beam deflections were calculated only at the load point. The analysis of the rib stress and deflection was made using simple beam theory with no attempt made to include the effects of transverse load distribution.

The loads were calculated in terms of a unit load "P". The external load equilibrium was obtained using a conventional analysis for indeterminate structures. The applied loads, shears, and moments are shown in Fig. 35.

During the tests small amounts of upward deflection were measured and are given below expressed as coefficients of the applied load "P".

flanged specimen: $\Delta = 0.975\ P \times 10^{-3}$ in.

unflanged specimen: $\Delta = 0.864\ P \times 10^{-3}$ in.

In order to calculate the effects of the upward deflection on the entire specimen, a dummy load (P') was applied at point "C" that would deflect the point upward the amount measured during the test. The moments and shears produced by this load were then calculated and superimposed on the moments and shears previously calculated assuming unyielding supports.

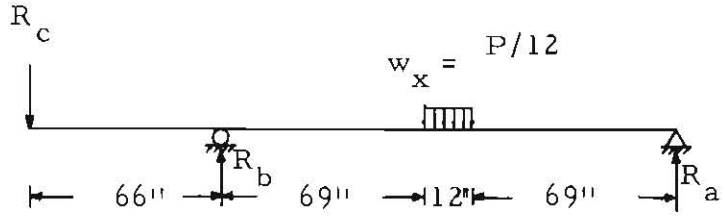

R_a = 0.370 P kips

R_b = 0.926 P kips

R_c = 0.296 P kips

w_x = P/12 kips/in

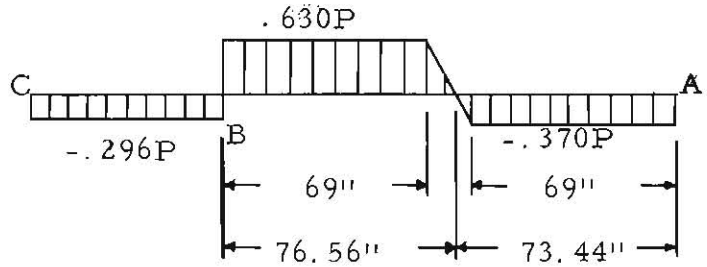

M_b = 19.56 P in-kip

M_{cl} = 26.25 P in-kip

M_{max} = 26.35P in-kip

$M_{1/4}$ = 13.88 P in-kip

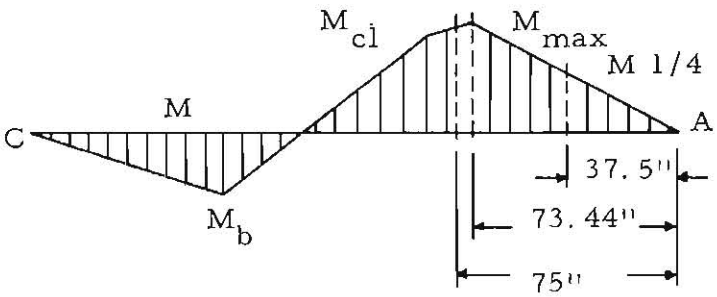

FIGURE 35. Loads, shear and moment produced by applied load.

The load at 'C' required to produce a unit deflection at 'C' is

$$P' = \frac{3EI\Delta}{a^2(L + a)} \qquad \text{where } a = 66 \text{ in. and } L = 150''$$

Therefore,

$$P' = \frac{(3)(29.6 \times 10^3)\, I\Delta}{(66)^2\,(150 + 66)} = 0.0944\, I\Delta \quad \text{kips}$$

The external load equilibrium, moments, and shears produced by this load are shown in Fig. 36.

Stresses are calculated on the lower (tension faces of the ribs at the load point and one-quarter point using the standard flexural formula of

$$\sigma = \frac{Mc}{I}$$

The stresses are calculated in Table V with values of c, I, and other section properties as given in Table III.

TABLE V. Flexural Stress

Location	Type Spec.	$\Delta \times 10^3$	I	c_1	$M_{P'}$	M_P	M	σ
Load point	flg	0.975P	576.2	9.07	1.75P	26.25P	28.00P	.441P
1/4 pt.	flg	0.975P	575.2	9.07	.87P	13.88P	14.75P	.233P
Load point	unf	0.864P	569.5	9.00	1.54P	26.25P	27.79P	.439P
1/4 pt.	unf	0.864P	569.5	9.00	.77P	13.88P	14.65P	.232P

The deflection of the specimen is calculated only at the load point. If local deformations are not considered, the total deflection will consist only of the flexural and shear deflection produced by both the applied load

LOADS

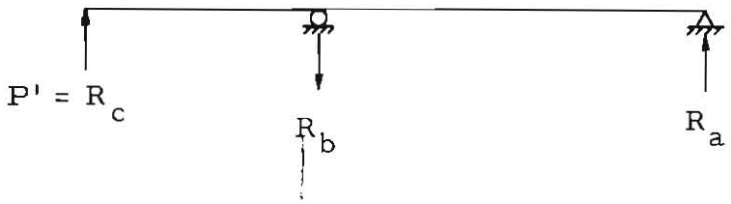

$R_a = .0415\ I\Delta$ kips

$R_b = .1359\ I\Delta$ kips

$P' = R = .0944\ I\Delta$ kips

SHEAR

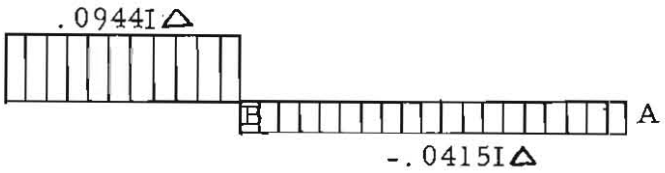

$M_b = 6.23\ I\Delta$ in-kips

$M_{cl} = 3.12\ I\Delta$ in-kips

$M_{l/4} = 1.561I\Delta$ in-kips

MOMENT

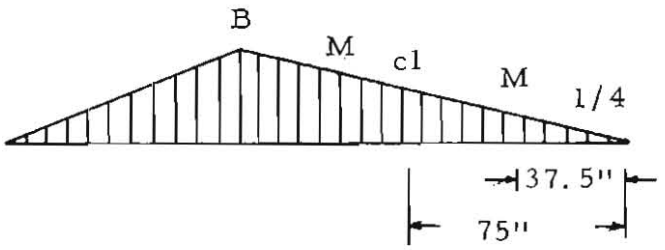

FIGURE 36. Loads, shear, and moment produced by support deflection.

and the upward deflection of the support at "C".

Flexural deflections can be more easily calculated if the external load equilibrium due to the applied loads is divided into two parts as shown in Fig. 37.

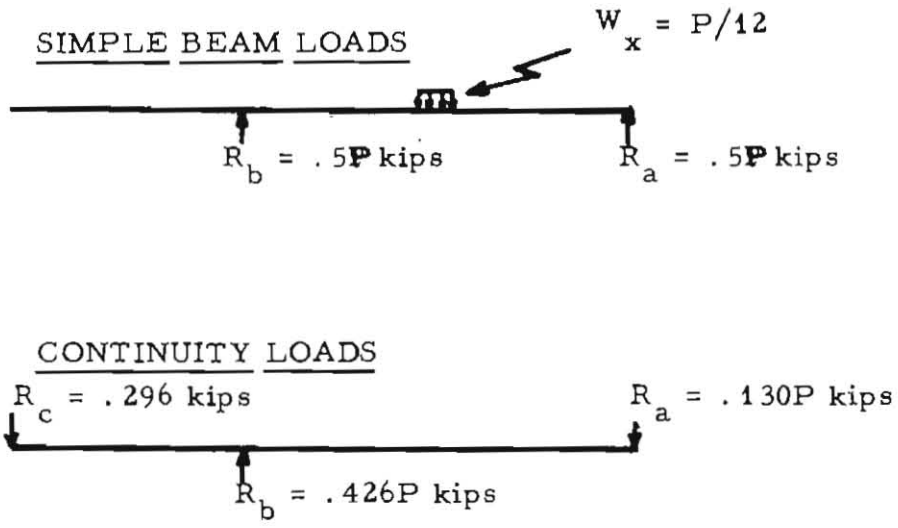

FIGURE 37. Loads-Unyielding Supports

The deflections produced by the continuity loads and the support movement are calculated separately from the deflections produced by simple beam loads.

The deflection due to simple beam loads can be calculated using the formula

$$y_{s'} = \frac{1}{48EI}\left\{8R_a(x^3 - L^2x) + P_x\left[\frac{8d^3}{L} - \frac{2bc_s^2}{L} - \frac{c_s^3}{L} + 2c_s^2\right] - 2P\frac{(x-a)^4}{c_s}\right\} = \frac{1}{48EI}\left\{8(P/2)(7.5-1.50^2 \cdot 75) + 75P\left[\frac{8(75)^3}{1.50}\right.\right.$$

$$- \frac{2(81 \times 12)^2}{150} + \frac{(12)3}{150} + 2(12)^2\Big] - 2P\frac{(75 - 69)^4}{12}\Bigg\}$$

Ref. 18

$$y_s = -\frac{70,500}{E} P$$

a = 69 in
b = 81 in
c_s = 12 in
d = x = 75 in
L = 150 in

The deflection at the load point produced by the continuity loads and support movement

$$y_c = \frac{P^*ax\,(L^2 - x^2)}{6EIL} = \frac{P^*(66)(75)(150^2 - 75^2)}{6EI\,150}$$

L = 150 in
a = 66 in
x = 75 in

$$P^* = (.296P - .0944I\,\Delta)$$

$$y_c = \frac{92210}{EI}(.296P - .0944\,\Delta)$$

The total flexural deflection is the sum of the two deflections.

$$y_f = y_c + y_s = \frac{-70,160P}{E3} + \frac{92,810}{EI}(.296P - .0944I\Delta)$$

$$y_c = \frac{-42,680P}{EI} - \frac{8,760\Delta}{E}$$

Deflections due to shear are calculated using a virtual work method.

$$y_{sh} = \lambda \int_0^L \frac{Vvdx}{A_s G}$$

The constant λ is assumed to be 1.0 and the shear area (A_s) is assumed to consist only of the area of the vertical portion of the rib walls (12.38 in^2). The shear diagram produced by a virtual load at the load point is shown in Fig. 38.

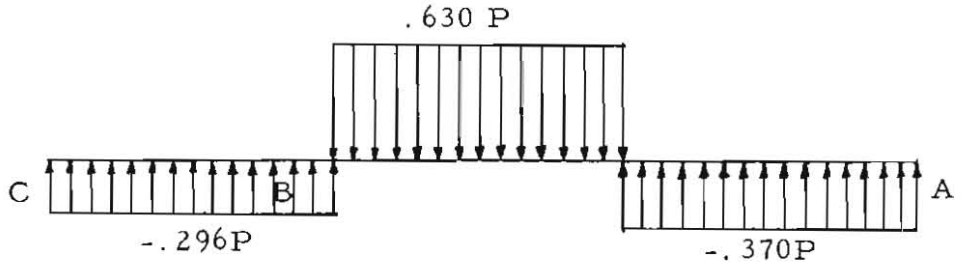

FIGURE 38. Virtual Load Shear

The shear diagram produced by the applied load "P", (Fig. 35) is simplified to have the same shape as the virtual load shear. Shear produced by the support deflection is shown in Fig. 36.

$$y_{sh} = \int_0^{75} \frac{(-0.370P - 0.0415I\Delta)(-0.370)dx}{A_s G} + \int_0^{75} \frac{(0.630P - 0.0415I\Delta)(0.630)dx}{A_s G}$$

$$+ \int_0^{66} \frac{(-0.296P + .0944I\Delta)(-0.296)dx}{A_s G}$$

$$= -\frac{1}{12.386}\left\{\left[.137Px + .015I\Delta x + .397Px = .026I\Delta x\right]_0^{75} + \left[.088Px - .028I\Delta x\right]_0^{66}\right\}$$

$$y_{sh} = 1/6\left[3.71P = .216I\Delta\right]$$

The total deflection is the linear combination of the shear and flexural deflection.

$$y = \left(\frac{-42,680P}{EI} - \frac{8760\Delta}{E}\right) + 1/G\left[-3.71P + .216I\right]$$

For the flanged specimen $I = 575.2\ in^4$

$\Delta = .975P \times 10^{-3}$ in

$$y_{flg} = \left[\frac{-42680P}{(29.6 \times 10^3)575.2} - \frac{(8760)(.975P \times 10^{-3})}{29.6 \times 10^3} \right]$$

$$+ \frac{1}{11.5 \times 10^3} \left[3.71P - .216(575.20)(.975 \times 10^{-3}) \right]$$

$$y_{flg} = \left[-2.50P - .30P - .32P + \text{neg.} \right] \; 10^{-3}$$

$$y_{flg} = -3.12P \times 10^{-3} \text{ in}$$

For the unflanged specimen: $I = 569.5$

$\Delta = .864P \times 10^{-3}$

$$y_{unf} = \left(\frac{-42,680}{(29.6 \times 10^3)(568.5)} - \frac{(8760)(.864P \times 10^{-3})}{29.6 \times 10^3} \right)$$

$$+ \frac{1}{11.5 \times 10^3} \left[3.71P - .216\,(569.5).864P \times 10^{-3} \right]$$

$$= \left[-2.53P - .26P - .32P \right] \times 10^{-3}$$

$$y_{unf} = -3.11P \times 10^{-3} \text{ in}$$

APPENDIX III
Local Stresses

The stresses under the load pad are calculated using a simplified method of analysis as compared with the method given in the AISC Manual (17). The analysis was made assuming that the deck plate has negligible torsional resistance as compared with the closed ribs. This allowed the rotation of the ribs to be calculated using simple torsion theory rather than by orthotropic plate theory. Only the maximum stress (6_{yy}) is calculated.

The loads were first distributed on a one inch strip assuming that the lower corners of the ribs do not deflect or rotate (Fig. 39). The actual transverse load distribution that exists under the load pad is highly indeterminate; however, it is reasonable to assume that most of the load is transmitted through the center eight inch portion of the load beam in which the bearing stiffners are located. The load distribution used (Fig. 39) attempts to represent this condition.

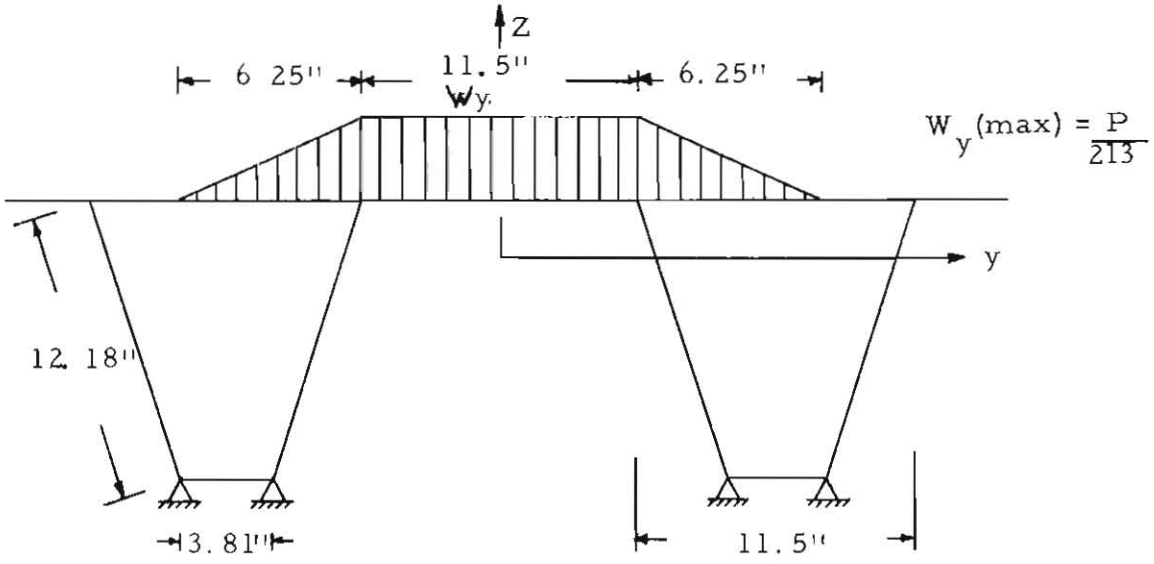

FIGURE 39. Load Distribution Model

The transverse moments, as obtained by moment distribution, are shown in Fig. 40.

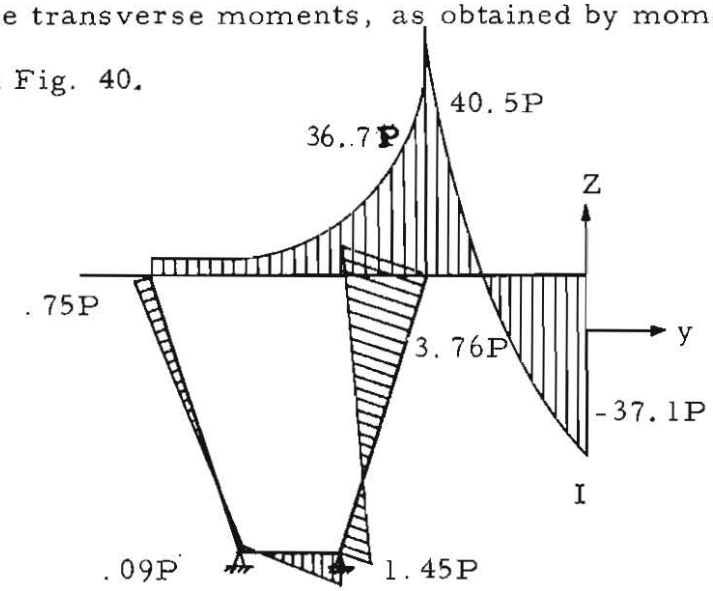

FIGURE 40. Moment

These moments must be modified to include the effect of load distribution in the longitudinal (x) direction. This is done using a plate factor " Ψ " (15). The plate factor for moment at the center line (y = 0)

$$\Psi = .71$$

The moment at the center line then is

$$M = (.71)(37.1P) = 26.4\ P \quad \text{in-kips}$$

The rib supports are then removed and the specimen allowed to deflect and rotate. As the deck is assumed to have no torsional stiffness, the ribs rotate independently of each other. The torque that rotates the rib is produced by the eccentricity of the load with the centerline of the rib (Fig. 41).

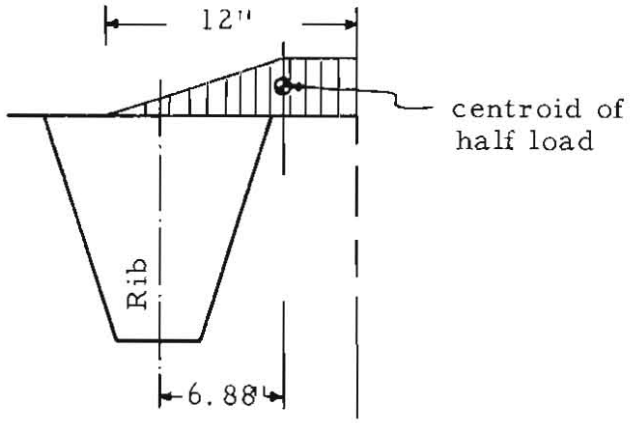

FIGURE 41. Applied Torque - Rib

The torque on each rib is then the product of the eccentricity times the half load or

$$T = (6.88)\, P/2 = 3.44P \quad \text{in-kips}$$

The basic load equilibrium used to determine the rib rotation is shown in Fig. 42.

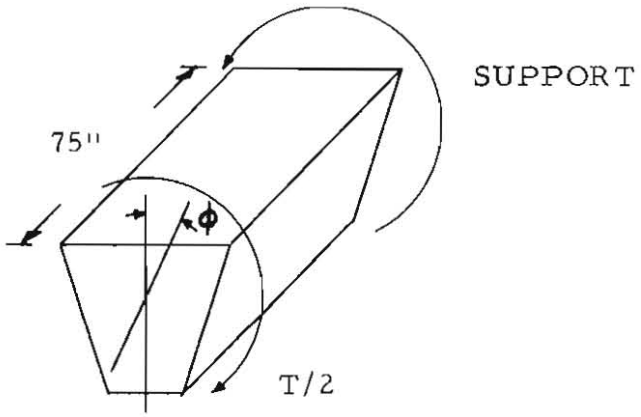

FIGURE 42. Load Equilibrium - Rib torque

The rib rotation is then calculated neglecting warping

$$\phi = \frac{(1/2)T\,(L/2)}{JG} = \frac{(1/2)(3.44P)\left(\frac{150}{2}\right)}{(229)(11.5 \times 10^{3})}$$

$J = 229 \text{ in}^4$ (Table III)

$L = 150$ in

$$\phi = 49.0 \times 10^{-6} P \text{ radians}$$

It is then assumed that the deck plate between the ribs must rotate the same amount as the rib, Fig. 43.

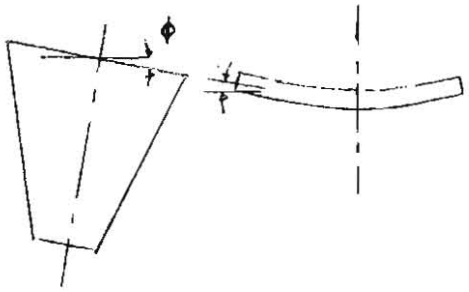

FIGURE 43. Deck Plate Rotation

The moment produced in the deck plate by the applied rotation is

$$M_{\phi} = \frac{2\phi EI_P}{l_p} = \frac{(49 \times 10^{-6}P)(29.6 \times 10^{6})(.00792)}{l_p}$$

$l_{p(unf)} = 11.5$ in

$l_{p(flg)} = 9.5$ in

$I_P = .00792$ in^4

$M_{\phi\ (unf)} = 2.0P$ in-kips

$M_{\phi\ (flg)} = 2.4P$ in-kips

The total transverse moment at the centerline of the load pad is the sum of the fixes moment and rotation moment.

$M_{d\ (unf)} = 26.4P + 2.0P = 28.4\ P$ in-kips

$M_{d\ (flg)} = 26.4P + 2.4P = 28.8\ P$ in-kips

Stresses produced by these moments are calculated using ordinary flexure theory

$$\sigma_{yy} = \frac{M_d c}{I_P} = \frac{M \frac{.456}{.26}}{.00792}$$

Unflanged $\sigma_{yy} = 8.18\ P$ ksi

Flanged $\sigma_{yy} = 8.29\ P$ ksi

The effects of beam flexure in the longitudinal direction must also be superimposed on the transverse deck stresses. The magnitude of the longitudinal compressive stress in the lower face of the deck can be calculated from Table V by changing the values of "c" to

$c_{unf} = -2.50$ in

$c_{flg} = -2.43$ in

and by using the moments given at the load point from the same table.

These compressive stresses are

$$\sigma_{xx} = \frac{Mc}{I}$$

Unflanged $\sigma_{xx} = \frac{(27.79P)(-2.50)}{569.5}$

Unflanged $\sigma_{xx} = -.122P$

Flanged $\sigma_{xx} = \frac{(28.0P)(-2.43)}{575.2}$

Flanged $\sigma_{xx} = -.118P$

The transverse stresses can then be calculated assuming a plane strain condition in the transverse direction ($\epsilon_y = 0$) and a plane stress condition in the vertical direction ($\sigma_z = 0$) Fig. 44.

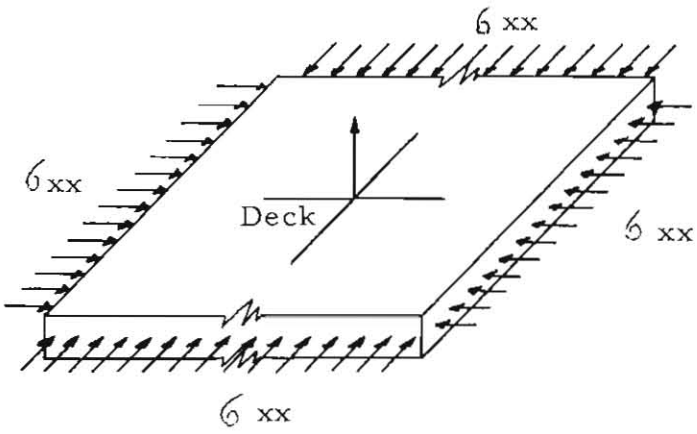

FIGURE 44.

The Hook's law equations for this condition ($\sigma_z = 0, \varepsilon_y = 0$) are

$$\varepsilon_x = 1/E(\sigma_x - \mu\sigma_y)$$

$$\varepsilon_y = 1/E(\sigma_y - \mu\sigma_x) = 0$$

$$\varepsilon_z = 1/E\left[-\mu(\sigma_x + \sigma_y)\right]$$

By manipulation, the stress in the transverse direction is found to be

$$\sigma'_{yy} = \mu\sigma'_{xx}$$

$$\sigma_{yy'} = .29\,\sigma_{xx'}$$

Unflanged $\sigma'_{yy} = .29\,(-.122P) = -0.03P$

Flanged $\sigma'_{yy} = (.29)(-.118P) = -0.03P$

The final transverse stress is then the summation of all the applied stresses.